

# FULLY DISCRETE ANALYSIS OF THE GALERKIN POD NEURAL NETWORK APPROXIMATION WITH APPLICATION TO 3D ACOUSTIC WAVE SCATTERING

JÜRGEN DÖLZ\* AND FERNANDO HENRÍQUEZ†

**Abstract.** In this work, we consider the approximation of parametric maps using the so-called Galerkin POD-NN method. This technique combines the computation of a reduced basis via proper orthogonal decomposition (POD) and artificial neural networks (NNs) for the construction of fast surrogates of said parametric maps. We provide a fully discrete error analysis of this method that accounts for different discretization errors, including the number of reduced basis in the approximation of the solution manifold, truncation in the parameter space, and, most importantly, the number of samples in the computation of the reduced space, together with the effect of the use of NNs in the approximation of the reduced coefficients. Following this error analysis we provide a-priori bounds on the required POD tolerance, the resulting POD ranks, and NN-parameters to maintain the order of convergence of quasi Monte Carlo sampling techniques.

The main advantage of Galerkin POD-NN over existing traditional techniques is that the online and offline phases of the projection-based reduced basis method are completely decoupled, making the evaluation of the constructed surrogate in run-time considerably faster without the need for an *hyper-reduction* technique.

We conclude this work by showcasing the applicability of this method through a practical industrial application: the sound-soft acoustic scattering problem by a parametrically defined scatterer in three physical dimensions.

## 1. Introduction.

**1.1. Motivation.** *Surrogate models* are key ingredients for the success of many-query applications where expensive computational models need to be repeatedly evaluated. Indeed, if the underlying model, obtained using standard discretization methods such as the Finite Element, Finite Volume, Finite Difference, or Boundary Element method (the latter for the numerical approximation of boundary integral equations, or BIEs), is computationally demanding, the repeated use of this model becomes cost-prohibitive.

A good surrogate model provides a fast approximation of the original problem, while guaranteeing a certified level of accuracy with respect to the so-called *high-fidelity* solution. Motivated by partial differential equations with random input data, inverse problems, and optimal control, the subject of this article are surrogate models to the *parameter-to-solution map* arising from parametric PDEs and BIEs.

More precisely, given Hilbert spaces  $\mathcal{X}, \mathcal{Y}$  and a compact subset  $\mathcal{U} \subset \mathcal{X}$ , referred as the *parameter space*, we consider the problem of finding for each in  $\nu \in \mathcal{U}$  the solution  $u(\nu) \in \mathcal{Y}$  to the following problem cast in variational form

$$(1.1) \quad \mathbf{a}(u(\nu), v; \nu) = \mathbf{f}(v; \nu), \quad \forall v \in \mathcal{Y},$$

where  $\mathbf{f}(\cdot; \nu) \in \mathcal{Y}'$ , and  $\mathbf{a}(\cdot, \cdot; \nu)$  represents in a general framework either a linear or non-linear PDE or BIE. Provided that (1.1) is well-posed for each input  $\nu \in \mathcal{U}$  one can define the *parameter-to-solution* map  $\mathcal{U} \ni \nu \mapsto u(\nu) \in \mathcal{Y}$ .

The construction of surrogate models to the (nonlinear) parameter-to-solution map given through (1.1) is obstructed by several issues. First, the infinite dimensionality of the parameter space requires appropriate truncation for numerical computa-

\*Institute for Numerical Simulation, University of Bonn, Friedrich-Hirzebruch-Allee 7, 53115 Bonn, Germany ([doelz@ins.uni-bonn.de](mailto:doelz@ins.uni-bonn.de)).

†Institute for Analysis and Scientific Computing, Vienna University of Technology, Wiedner Hauptstrae 8-10, A-1040 Wien, Austria. ([fernando.henriquez@asc.tuwien.ac.at](mailto:fernando.henriquez@asc.tuwien.ac.at)).

tions. Second, the variational problem can usually only be solved approximately by means of a Galerkin approach which often requires many degrees of freedom. And third, the solution manifold

$$(1.2) \quad \mathcal{M} := \{u(\nu) \in \mathcal{Y} : \nu \in \mathcal{U}\}$$

is itself infinite or high dimensional without any further measures.

The recent success of deep learning techniques in several fields of science and engineering has led to many works suggesting the use *artificial neural networks* in the approximation of the parameter-to-solution map, a growing field referred to as *Operator Learning* or *Neural Operators*.

**1.2. Related work.** The so-called “training” of plain vanilla neural networks can be interpreted as solving a non-linear regression problem, i.e., to fit the parameters of a specific non-linear function  $\mathbb{R}^N \rightarrow \mathbb{R}^M$  (in this case the neural network) such that a loss functional is minimized [4, 24]. It is well known that neural networks allow for universal approximation of properties, that is, they can approximate certain function classes up to arbitrary accuracy as long as the network is wide enough; see, e.g., [5, 11, 16, 37, 52]. Many results provide guaranteed convergence rates [15, 14, 33, 59], with a particular focus on beating the so-called *curse of dimensionality* in the parameter space.

However, using NNs to approximate the parameter-to-solution map requires architectures that account for the high, or even infinite, dimensionality of both the input and output spaces. In the last years, several of these have been proposed, e.g. DeepONets [47, 43, 42, 55, 62], Fourier Neural Operators [25, 39, 44], graph neural operator [53], convolutional neural operators [23, 57], and PCA-nets [3, 34, 36, 41, 59]. The latter is also known as the Galerkin POD-NN, and is the focus of this work. Though not the framework considered in this work, we mention in passing that the Galerkin POD-NN has been extended to time-dependent problems, see e.g. [26, 60, 61].

In order to appropriately deal with the parameter-to-solution map  $\mathcal{U} \ni \nu \mapsto u(\nu) \in \mathcal{Y}$  and effectively build a suitable method that leverages on NNs for its approximation, the complexity of both the input and output spaces needs to be appropriately described by a *encoder-decoder* pair. That is, we construct maps  $\mathcal{E} : \mathcal{U} \rightarrow \mathbb{R}^N$ ,  $\boldsymbol{\pi} : \mathbb{R}^N \rightarrow \mathbb{R}^M$ , and  $\mathcal{D} : \mathbb{R}^M \rightarrow \mathcal{M}$  such that

$$(1.3) \quad \mathcal{X} \supset \mathcal{U} \xrightarrow{\text{Encoder } \mathcal{E}} \mathbb{R}^N \xrightarrow{\text{Neural Network } \boldsymbol{\pi}} \mathbb{R}^M \xrightarrow{\text{Decoder } \mathcal{D}} \mathcal{M} \subset \mathcal{Y}.$$

Then, for each input  $\nu \in \mathcal{U}$  one can construct an approximation of the parameter-to-solution map which reads as  $u(\nu) \approx (\mathcal{D} \circ \boldsymbol{\pi} \circ \mathcal{E})(\nu)$ . Indeed, the task of operator learning boils down to defining the encoder-decoder pair and computing an appropriate NN  $\boldsymbol{\pi}$ . This NN is of hopefully moderate size. This is understood not only in the sense that  $N$  and  $M$  are controlled, but also in terms of the overall network size, which is determined by the number of trainable parameters.

The Galerkin POD-NN method relies on the combination of projection-based model order reduction techniques for the construction of the decoder, in particular, the reduced basis method [35, 56] and, of course, NNs. The reduced basis method, which is at the core of the methodology presented here, follows a two phase paradigm—online and offline—for the swift and efficient evaluation of the parameter-to-solution map. In the offline phase, a basis of reduced dimension is computed by properly sampling the space  $\mathcal{U}$  and performing a proper orthogonal decomposition (POD), although *greedy* strategies could also be put in place. These allow for the identification of the most

important modes driving the dynamics of the parameter-to-solution map. Next, in the online phase, the evaluation of the parameter-to-solution map for a given parametric input is computed in a variational fashion as an element of the reduced space. For this purpose, hyper-reduction techniques, such as the empirical interpolation method [2] and its discrete counterpart [6], can be used. However, these techniques are intrusive in nature, and their implementation is not trivial. Instead, the idea of the Galerkin-POD NN, originally pointed out in [36], is to use a NN for the approximation of the reduced coefficients, i.e. for the computation of the central part in (1.3). This completely decouples the online and offline phases, and makes the approximation of the reduced coefficients purely *data-driven*.

Summarized, the Galerkin-POD NN provides an *algorithmically implementable* and *computationally feasible* construction of the decoder. What remains to be understood is the interplay of the approximation errors of the neural network approximation, the Galerkin-POD, and the Galerkin approximation to the variational problem and how to balance them to obtain an accurate and computationally efficient approximation scheme.

**1.3. Contributions.** The goal of this paper is to provide fully discrete a-priori approximation rates of the neural network approximation of parameter-to-solution maps to (1.1) which account for all approximation errors occurring in *algorithmically feasible* computations. To this end, we consider the Galerkin POD-NN architecture when the parameter-to-solution map and its Galerkin approximation are  $(\mathbf{b}, p, \varepsilon)$ -holomorphic and the samples are drawn according to quasi-Monte Carlo (QMC) rules, as for example suggested in [46, 48, 49]. For this setting we

- (i) Provide a-priori approximation rates for the Galerkin POD reduced basis which account for truncation in the parameter space, the Galerkin-error for (1.1), and the sampling error in the high-dimensional parameter space.
- (ii) Provide a-priori approximation rates for the *algorithmically implementable* and *computationally feasible* Galerkin POD-NN using tanh NNs up to the training error with dimension-robust convergence rates.
- (iii) Demonstrate the validity of our approximation estimates on an industrially relevant application: acoustic wave scattering by random domains in three spatial dimensions.

**1.4. Outline.** This work is structured as follows. In section 2 we recall important concepts concerning the analytic smoothness of the parametric maps under consideration upon the parametric inputs. In addition, we recall the projection-based MOR and, in particular, the reduced basis method. In section 3, we provide a complete error analysis for the Galerkin-POD method. In section 4 we formally introduce NNs and provide a complete error analysis for the approximation of the Galerkin-POD NN. In section 5 we introduce the model problem to be considered for the numerical experiments. We conclude this work by presenting a set of numerical experiments in section 6 and provide some final remarks in section 7.

**2. Parametric Problems and projection-based MOR.** In this section, we recall important aspects concerning parametric PDEs, parametric holomorphy, and the so-called projection-based *model-order reduction (MOR)*, in particular the reduced basis method.

**2.1. Encoder-decoder construction.** Firstly, we discuss the construction of both the encoder and decoder in our approach. For the former, loosely speaking, we assume that each element of the parameter space  $\mathcal{U}$  can be represented through a

sequence of real numbers. More precisely, we set  $\mathbb{U} := [-1, 1]^{\mathbb{N}}$  and assume that for each element of  $\nu \in \mathcal{U} \subset \mathcal{X}$  there exists  $\mathbf{y} \in \mathbb{U}$  such that  $\nu = T(\mathbf{y})$ , where  $T : \mathbb{U} \mapsto \mathcal{U}$ .

Typically, the map is chosen to be affine with respect to the parametric input, i.e. it is of the form

$$(2.1) \quad T(\mathbf{y}) = \nu_0 + \sum_{j \geq 1} y_j \nu_j \in \mathcal{U}, \quad \mathbf{y} \in \mathbb{U}, \quad \{\|\nu_j\|_{\mathcal{X}}\}_{j \in \mathbb{N}} \in \ell^1(\mathbb{N}),$$

where  $\{\nu_0, \nu_1, \dots\} \subset \mathcal{X}$ , together with its dimension-truncated counterpart

$$(2.2) \quad T_s(\mathbf{y}) = \nu_0 + \sum_{j=1}^s y_j \nu_j \in \mathcal{U}, \quad \mathbf{y} \in \mathbb{U}^{(s)}.$$

As discussed in [8, Section 1.2], for the case of  $\mathcal{X}$  a Banach space and  $\mathcal{U}$  a compact subset, it can be proven that maps  $T$  of the form described in (2.1) do indeed exist. However, as discussed therein this representation might not be unique and not every element of  $\mathcal{U}$  might admit one. This issue is, for example, addressed in [34] by resorting to frames and Riesz bases in the construction of representation of the form (2.1).

Furthermore, in the statistical context and under the assumption that  $\mathcal{X}$  is a Hilbert space, an expansion can be constructed as in (2.1) using the Karhunen–Loève theorem [45], which is indeed the approach that we follow in the application presented in section 5. Herein, we assume that  $\mathcal{U} := \{\nu = T(\mathbf{y}) : \mathbf{y} \in \mathbb{U}\}$  and that  $\{\nu_0, \nu_1, \dots\}$  form a basis of  $\mathcal{U}$ , thus rendering the encoder

$$(2.3) \quad \mathcal{E}(\nu) = T^{-1}(\nu)$$

well-defined. For the construction of the decoder, as extensively discussed in subsection 1.2 we use a reduced basis  $\{\zeta_1^{(\text{rb})}, \dots, \zeta_M^{(\text{rb})}\}$  of dimension  $M$  constructed using the POD approach. Then, the decoder is reads as follows

$$(2.4) \quad \mathcal{D}(x) := \sum_{i=1}^M x_i \zeta_i^{(\text{rb})}, \quad x = \{x_i\}_{i=1}^M.$$

The remainder of this section is dedicated to the computational construction of such a reduced basis for parametrically holomorphic maps.

**2.2. Parametric holomorphy.** Recall that  $\mathbb{U} := [-1, 1]^{\mathbb{N}}$  and equip it with the product topology. For  $s > 1$  we define the Bernstein ellipse

$$(2.5) \quad \mathcal{E}_s := \left\{ \frac{z + z^{-1}}{2} : 1 \leq |z| \leq s \right\} \subset \mathbb{C}.$$

This ellipse has foci at  $z = \pm 1$  and semi-axes of length  $a := (s + s^{-1})/2$  and  $b := (s - s^{-1})/2$ . In addition, we define the tensorized poly-ellipse

$$(2.6) \quad \mathcal{E}_{\boldsymbol{\rho}} := \bigotimes_{j \geq 1} \mathcal{E}_{\rho_j} \subset \mathbb{C}^{\mathbb{N}},$$

where  $\boldsymbol{\rho} := \{\rho_j\}_{j \geq 1}$  is such that  $\rho_j > 1$ , for  $j \in \mathbb{N}$ .

**DEFINITION 2.1** ([7, Definition 2.1]). *Let  $X$  be a complex Banach space equipped with the norm  $\|\cdot\|_X$ . For  $\varepsilon > 0$  and  $p \in (0, 1)$ , we say that map  $\mathbb{U} \ni \mathbf{y} \mapsto u(\mathbf{y}) \in X$  is  $(\mathbf{b}, p, \varepsilon)$ -holomorphic if and only if:*

1. The map  $\mathbb{U} \ni \mathbf{y} \mapsto u(\mathbf{y}) \in X$  is uniformly bounded.
2. There exists a positive sequence  $\mathbf{b} := \{b_j\}_{j \geq 1} \in \ell^p(\mathbb{N})$  and a constant  $C_\varepsilon > 0$  such that for any sequence  $\boldsymbol{\rho} := \{\rho_j\}_{j \geq 1}$  of numbers strictly larger than one that is  $(\mathbf{b}, \varepsilon)$ -admissible, i.e. satisfying  $\sum_{j \geq 1} (\rho_j - 1)b_j \leq \varepsilon$ , the map  $\mathbf{y} \mapsto u(\mathbf{y})$  admits a complex extension  $\mathbf{z} \mapsto u(\mathbf{z})$  that is holomorphic with respect to each variable  $z_j$  on a set of the form

$$(2.7) \quad \mathcal{O}_\rho := \bigotimes_{j \geq 1} \mathcal{O}_{\rho_j},$$

where

$$(2.8) \quad \mathcal{O}_{\rho_j} = \{z \in \mathbb{C} : \text{dist}(z, [-1, 1]) < \rho_j - 1\}.$$

3. This extension is bounded on  $\mathcal{E}_\rho$  according to

$$(2.9) \quad \sup_{\mathbf{z} \in \mathcal{E}_\rho} \|u(\mathbf{z})\|_X \leq C_\varepsilon.$$

**2.3. Model Problem: Parametric Variational Problems.** Let  $X$  be a complex Hilbert space equipped with the inner product  $(\cdot, \cdot)_X$ , induced norm  $\|\cdot\|_X$ , and with the associated Banach space of continuous sesquilinear forms

$$(2.10) \quad B(X) = \{\mathbf{a} : X \times X \rightarrow \mathbb{C} : \|\mathbf{a}\|_{\text{op}} < \infty\}$$

equipped with the norm

$$(2.11) \quad \|\mathbf{a}\|_{\text{op}} := \sup_{v, w \in X \setminus \{0\}} \frac{|\mathbf{a}(v, w)|}{\|v\|_X \|w\|_X}.$$

For each  $\mathbf{y} \in \mathbb{U}$ , we consider the parameterized variational problem of finding  $u(\mathbf{y}) \in X$  such that

$$(2.12) \quad \mathbf{a}(u(\mathbf{y}), v; \mathbf{y}) = f(v; \mathbf{y}), \quad \forall v \in X,$$

where  $f(\cdot; \mathbf{y}) \in X'$  and  $\mathbf{a}(\cdot, \cdot; \mathbf{y}) \in B(X)$ . We assume  $f(\cdot; \mathbf{y})$  and  $\mathbf{a}(\cdot, \cdot; \mathbf{y})$  to be uniformly continuous, i.e., to satisfy

$$(2.13) \quad |f(v; \mathbf{y})| \leq \gamma \|v\|_X, \quad \forall v \in X, \quad \mathbf{y} \in \mathbb{U},$$

and

$$(2.14) \quad |\mathbf{a}(u, v; \mathbf{y})| \leq \bar{\alpha} \|u\|_X \|v\|_X, \quad \forall u, v \in X, \quad \mathbf{y} \in \mathbb{U},$$

we assume  $\mathbf{a}(\cdot, \cdot; \mathbf{y})$  to be uniformly inf-sup stable, i.e., to satisfy

$$(2.15) \quad \inf_{u \in X} \sup_{v \in X} \frac{|\mathbf{a}(u, v; \mathbf{y})|}{\|u\|_X \|v\|_X} \geq \underline{\alpha}, \quad \forall u, v \in X, \quad \mathbf{y} \in \mathbb{U},$$

for some constants  $\gamma \in (0, \infty)$  and  $0 < \underline{\alpha} \leq \bar{\alpha} < \infty$  which are independent of  $\mathbf{y}$ , and we assume that for all  $v \in X \setminus \{0\}$ ,  $\mathbf{y} \in \mathbb{U}$ , there exists  $u \in X$  such that  $\mathbf{a}(u, v; \mathbf{y}) \neq 0$ . Under these conditions, the Babuška-Aziz theorem implies that for each  $\mathbf{y} \in \mathbb{U}$  there exists a bounded solution operator  $\mathcal{S}(\cdot, \mathbf{y}) : X' \rightarrow X$  for each  $\mathbf{y} \in \mathbb{U}$  with operator norm uniformly bounded on  $\mathbb{U}$ .

For the Galerkin discretization of (2.12) let  $\{X_h\}_{h>0} \subset X$  be a sequence of one-parameter finite-dimensional subspaces that are densely embedded in  $X$ . The discrete variational formulation of (2.12) is then to find  $u_h(\mathbf{y}) \in X_h$  such that

$$(2.16) \quad \mathbf{a}(u_h(\mathbf{y}), v_h; \mathbf{y}) = \mathbf{f}(v_h; \mathbf{y}), \quad \forall v_h \in X_h.$$

We note that  $\mathbf{a}(\cdot, \cdot; \mathbf{y})$  and  $\mathbf{f}(\cdot; \mathbf{y})$  are uniformly continuous on  $X_h \subset X$  with the same constants as in (2.13) and (2.14) and assume  $\mathbf{a}(\cdot, \cdot; \mathbf{y})$  to be uniformly inf-sup stable on  $X_h$ , i.e., we assume that it holds

$$(2.17) \quad \inf_{w_h \in X_h} \sup_{v_h \in X_h} \frac{\mathbf{a}(w_h, v_h; \mathbf{y})}{\|w_h\|_X \|v_h\|_X} \geq \alpha, \quad \mathbf{y} \in \mathbb{U},$$

with (without loss of generality) the same constant as in (2.14), which is independent of the discretization parameter  $h$ . We further assume that for all  $v_h \in X_h \setminus \{0\}$ ,  $\mathbf{y} \in \mathbb{U}$ , there exists  $u_h \in X_h$  such that  $\mathbf{a}(u_h, v_h; \mathbf{y}) \neq 0$ . Again, the Babuška-Azis theorem implies that for each  $\mathbf{y} \in \mathbb{U}$  there exists a discrete solution operator  $\mathbf{S}_h(\cdot, \mathbf{y}): X' \rightarrow X_h$  for each  $\mathbf{y} \in \mathbb{U}$  whose operator norms are uniformly bounded on  $\mathbb{U}$  by the same constant as for the continuous case.

Moreover, we in the following we assume that

$$(2.18) \quad \mathbf{a}: \mathbb{U} \rightarrow B(X), \quad \mathbf{f}: \mathbb{U} \rightarrow X'$$

are  $(\mathbf{b}, p, \varepsilon)$ -holomorphic and continuous mappings in the sense of Definition 2.1. The assumptions then imply that the *parameter-to-solution map*  $\mathbf{y} \mapsto u(\mathbf{y})$  defined through (2.12) and the *discrete parameter-to-solution map*  $\mathbf{y} \mapsto u_h(\mathbf{y})$  defined through (2.16) are also  $(\mathbf{b}, p, \varepsilon)$ -holomorphic and continuous, see, e.g., [7].

**2.4. Proper Orthogonal Decomposition.** Usually, the numerical approximation of  $u_h(\mathbf{y}) \in X_h$  for each instance of the parametric input  $\mathbf{y} \in \mathbb{U}$  is computationally demanding, thus rendering any application that requires a repeated evaluation of the parameter-to-solution map prohibitively expensive.

Consider the *discrete solution manifold*

$$(2.19) \quad \mathcal{M}_h := \{u_h(\mathbf{y}) : \mathbf{y} \in \mathbb{U}\} \subset X_h.$$

We aim to approximate  $\mathcal{M}_h$  by low-dimensional linear subspaces following the reduced basis method, see, e.g., [51, 56] and the references therein. More precisely, we seek a  $J$ -dimensional subspace  $X_{h,J} \subset X_h$  minimizing the projection error in the  $L^2(\mathbb{U}; X)$  sense, i.e.

$$(2.20) \quad X_{h,J}^{(\text{rb})} = \arg \min_{\substack{X_{h,J} \subset X_h \\ \dim X_{h,J} \leq J}} \varepsilon_h(X_{h,J}),$$

where

$$(2.21) \quad \varepsilon_h(X_{h,J}) := \|u_h - \mathbf{P}_{X_{h,J}} u_h\|_{L^2(\mathbb{U}; X)}^2 = \int_{\mathbf{y} \in \mathbb{U}} \|u_h(\mathbf{y}) - \mathbf{P}_{X_{h,J}} u_h(\mathbf{y})\|_X^2 \mu(d\mathbf{y}).$$

Therein, we define the operator  $\mathbf{P}_{X_{h,J}} : X \rightarrow X_{h,J}$  as the orthogonal projection operator onto  $X_{h,J}$  with respect to  $(\cdot, \cdot)_X$  and introduce the following tensor product uniform measure in  $\mathbb{U}$

$$(2.22) \quad \mu(d\mathbf{y}) = \bigotimes_{j \in \mathbb{N}} \frac{dy_j}{2}.$$

We also note that [Item 1](#) in the definition of the  $(\mathbf{b}, p, \varepsilon)$ -holomorphy implies that  $u_h \in L^2(\mathbb{U}; X_h)$ , and that the operators

$$(2.23) \quad \mathbb{T}_h: L^2(\mathbb{U}) \rightarrow X_h, \quad g \mapsto \mathbb{T}_h g = \int_{\mathbb{U}} u_h(\mathbf{y}) g(\mathbf{y}) \mu(d\mathbf{y}),$$

$$(2.24) \quad \mathbb{T}_h^*: X_h \rightarrow L^2(\mathbb{U}), \quad x \mapsto \mathbb{T}_h^* x = (u_h(\mathbf{y}), x)_X$$

are Hilbert-Schmidt ones, and thus compact. This makes the integral operator

$$(2.25) \quad \mathbb{K}_h: X_h \rightarrow X_h, \quad x \mapsto \mathbb{K}_h x = \mathbb{T}_h \mathbb{T}_h^* x = \int_{\mathbb{U}} u_h(\mathbf{y}) (u_h(\mathbf{y}), x)_X \mu(d\mathbf{y}),$$

compact, self-adjoint, and positive definite. Consequently, it has a countable sequence of eigenpairs  $(\zeta_{h,i}, \sigma_{h,i}^2)_{i=1}^r \in X \times \mathbb{R}_{\geq 0}$ , being  $r \in \mathbb{N}$  the rank of the operator  $\mathbb{T}_h$ , with the eigenvalues accumulating at zero. In the following, we assume that  $\sigma_{h,1} \geq \sigma_{h,2} \geq \dots \geq \sigma_{h,r} \geq 0$ . Moreover, it is well-known that the span of the eigenfunctions to the  $J$  largest eigenvalues, referred to as *reduced basis*,

$$(2.26) \quad X_{h,J}^{(\text{rb})} = \text{span} \{ \zeta_{h,1}, \dots, \zeta_{h,J} \} \subset X_h,$$

minimizes the projection error [\(2.21\)](#), that is in the  $L^2(\mathbb{U}; X_h)$  sense, among all  $J$ -dimensional subspaces of  $X_h$  of dimension at most  $J$  to

$$(2.27) \quad \varepsilon_h \left( X_{h,J}^{(\text{rb})} \right) = \sum_{i=J+1}^r \sigma_{h,i}^2.$$

Recall that for a compact subset  $\mathcal{K}$  of a Banach space  $X$  the Kolmogorov's width is defined for  $L \in \mathbb{N}$  as

$$(2.28) \quad d_J(\mathcal{K}, X) := \inf_{\dim(X_J) \leq J} \sup_{v \in \mathcal{K}} \min_{w \in X_J} \|v - w\|_X,$$

where the outer infimum is taken over all finite dimensional subspaces of dimension at most  $J$ .

Considering that in our case  $X$  is a Hilbert space, one can readily observe that  $\sqrt{\varepsilon \left( X_{h,J}^{(\text{rb})} \right)} \leq d_J(\mathcal{M}_h, X_h)$  and recalling, e.g., [\[9\]](#) one may conclude that

$$(2.29) \quad \varepsilon_h \left( X_{h,J}^{(\text{rb})} \right) \lesssim J^{-2\left(\frac{1}{p}-1\right)},$$

with an implicit constant independent of  $h > 0$  and  $J$ .

**2.5. Empirical POD.** The construction of the reduced basis  $X_{h,J}^{(\text{rb})}$  introduced in [\(2.26\)](#) as described in [subsection 2.4](#) is not feasible in practice as  $\mathbb{K}_h$  is not computationally accessible. To overcome this issue, one seeks a  $J$ -dimensional subspace

$$(2.30) \quad X_{h,s,N,J}^{(\text{rb})} = \arg \min_{\substack{X_{h,J} \subset X_h \\ \dim X_{h,J} \leq J}} \varepsilon_{h,s,N}(X_{h,J}),$$

which is the unique minimizer of the *computable or empirical* error measure

$$(2.31) \quad \varepsilon_{h,s,N}(X_J) := \frac{1}{N} \sum_{n=1}^N \left\| u_h \left( \mathbf{y}^{(n)} \right) - \mathbb{P}_{X_J} u_h \left( \mathbf{y}^{(n)} \right) \right\|_X^2,$$

with sample points  $\{\mathbf{y}^{(n)}\}_{n=1}^N \subset \mathbb{U}^{(s)} := [-1, 1]^s$ ,  $s \in \mathbb{N}$ . Similarly to  $\mathbb{U}$ , we equip  $\mathbb{U}^{(s)}$  with the structure of a probability space and with the tensor product unit measure

$$(2.32) \quad \mu^s(d\mathbf{y}) = \bigotimes_{j=1}^s \frac{dy_j}{2}.$$

Without going into further details we write  $\mathbb{U}^{(s)} \hookrightarrow \mathbb{U}$ , referring to an extension of coefficient vectors by zero. We assume that these sample points are taken to be quasi-Monte Carlo points such as the Halton point sequences [27] or higher order quasi-Monte Carlo based on IPL sequences, see e.g. [17, 18, 19].

We further assume to have a basis  $\{\varphi_1, \dots, \varphi_{N_h}\}$  of  $X_h$  to our disposal and denote by boldface letters  $\mathbf{w}_h \in \mathbb{C}^{N_h}$  the coefficients vector of a functions  $w_h \in X_h$  in the aforementioned basis. Using the mass matrix  $\mathbf{M}_h \in \mathbb{R}^{N_h \times N_h}$  defined as

$$(2.33) \quad (\mathbf{M}_h)_{i,j} = (\varphi_i, \varphi_j)_X, \quad i, j \in \{1, \dots, N_h\},$$

this one-to-one correspondence yields finite dimensional representations of norm and inner product in  $X_h$ , which read

$$(2.34) \quad (v_h, w_h)_X = \mathbf{v}_h^* \mathbf{M}_h \mathbf{w}_h \quad \text{and} \quad \|v_h\|_X = \sqrt{\mathbf{v}_h^* \mathbf{M}_h \mathbf{v}_h} =: \|\mathbf{v}_h\|_{\mathbf{M}_h},$$

for  $v_h, w_h \in X_h$ . We recall that  $\mathbf{M}_h$  is symmetric and positive definite.

Let  $X_{h,J}$  be a subspace of  $X_h$  of dimension  $J$  which is spanned by the orthonormal basis  $\{v_h^{(1)}, \dots, v_h^{(J)}\}$ . Set  $\Phi = \left( \mathbf{v}_h^{(1)}, \dots, \mathbf{v}_h^{(J)} \right)$  where each  $\mathbf{v}_h^{(i)} \in \mathbb{C}^{N_h}$  collects the coefficients of the representation of  $v_h^{(i)}$  in the basis  $\{\varphi_1, \dots, \varphi_{N_h}\}$  of  $X_h$ . Using these facts, (2.31) becomes an algorithmically implementable error measure

$$(2.35) \quad \begin{aligned} \varepsilon_{h,s,N}(X_{h,J}) &= \frac{1}{N} \sum_{n=1}^N \left\| \mathbf{u}_h(\mathbf{y}^{(n)}) - \sum_{j=1}^J \left( (\mathbf{v}_h^{(j)})^* \mathbf{M}_h \mathbf{u}_h(\mathbf{y}^{(n)}) \right) \mathbf{v}_h^{(j)} \right\|_{\mathbf{M}_h}^2 \\ &= \frac{1}{N} \sum_{n=1}^N \left\| \mathbf{u}_h(\mathbf{y}^{(n)}) - \Phi \Phi^* \mathbf{M}_h \mathbf{u}_h(\mathbf{y}^{(n)}) \right\|_{\mathbf{M}_h}^2. \end{aligned}$$

To compute the minimum of this error measure we define the *snapshot matrix* as

$$(2.36) \quad \tilde{\mathbf{S}} := \left( \mathbf{u}_h(\mathbf{y}^{(1)}), \dots, \mathbf{u}_h(\mathbf{y}^{(N)}) \right) \in \mathbb{C}^{N_h \times N},$$

where, as previously explained, each  $\mathbf{u}_h(\mathbf{y}^{(i)})$  corresponds to the representation in the basis of  $X_{h,J}$  of  $u_h(\mathbf{y}^{(i)})$ . Considering the SVD  $\mathbf{S} = \mathbf{U} \mathbf{\Sigma} \mathbf{V}^\dagger$  of  $\mathbf{S} = N^{-1/2} \mathbf{M}_h^{1/2} \tilde{\mathbf{S}}$ , where

$$(2.37) \quad \mathbf{U} = (\boldsymbol{\zeta}_1, \dots, \boldsymbol{\zeta}_{N_h}) \in \mathbb{R}^{N_h \times N_h}, \quad \mathbf{V} = (\boldsymbol{\psi}_1, \dots, \boldsymbol{\psi}_{N_h}) \in \mathbb{R}^{N \times N},$$

are orthogonal matrices and  $\mathbf{\Sigma} = \text{diag}(\sigma_{h,1}, \dots, \sigma_{h,\tilde{r}}) \in \mathbb{R}^{N_h \times N}$  with  $\sigma_{h,1} \geq \dots \geq \sigma_{h,\tilde{r}} > 0$ , being  $\tilde{r} \in \mathbb{N}$  the rank of  $\tilde{\mathbf{S}}$ , we obtain through POD the following basis of reduced dimension  $J$

$$(2.38) \quad \Phi_J^{(\text{rb})} = \left( \boldsymbol{\zeta}_1^{(\text{rb})}, \dots, \boldsymbol{\zeta}_J^{(\text{rb})} \right) = \left( \mathbf{M}_h^{-1/2} \boldsymbol{\zeta}_1, \dots, \mathbf{M}_h^{-1/2} \boldsymbol{\zeta}_J \right)$$



for  $J \leq \tilde{r}$ . This basis is such that its span understood as elements of  $X_h$ , which in the following we refer to as  $X_{N,s,h,J}^{(\text{rb})}$ , satisfies

$$(2.39) \quad \varepsilon_{h,s,N} \left( X_{h,s,N,J}^{(\text{rb})} \right) = \min_{\substack{X_{h,J} \subset X_h \\ \dim X_{h,J} \leq J}} \varepsilon_{h,s,N} \left( X_{h,J} \right) = \sum_{i=J+1}^{\tilde{r}} \sigma_{h,i}^2,$$

see, e.g., [56, Proposition 6.2].

REMARK 1. *Rather than applying  $\mathbf{M}_h^{\pm 1/2}$ , in actual computations one would evaluate*

$$(2.40) \quad \mathbf{C} = \frac{1}{N} \tilde{\mathbf{S}}^* \mathbf{M}_h \tilde{\mathbf{S}},$$

exploit that  $\mathbf{C}\boldsymbol{\psi}_i = \mathbf{S}^* \mathbf{S} \boldsymbol{\psi}_i = \sigma_i^2 \boldsymbol{\psi}_i$ , compute the eigenpairs corresponding to the  $J$  largest eigenvalues of  $\mathbf{C}$ , and set  $\boldsymbol{\zeta}_i = \sigma_i^{-1} \mathbf{S} \boldsymbol{\psi}_i$ ,  $i = 1, \dots, J$ , see also [56].

**3. Fully Discrete Analysis of the Galerkin-POD RB Method.** In this section, we provide a complete error analysis of the Galerkin-POD RB method.

**3.1. Galerkin POD Error Estimate.** The goal of this section is to bound the error between the solution  $u$  to (2.12) and  $\mathbf{P}_{X_{h,s,N,J}^{(\text{rb})}} u_h$  with  $X_{h,s,N,J}^{(\text{rb})}$  as in (2.39) and  $u_h$  as in (2.16) in terms of the following error sources and corresponding discretization variables: (i) Galerkin discretization ( $h > 0$ ), (ii) dimension truncation of the parametric input ( $s \in \mathbb{N}$ ), (iii) reduced basis approximation ( $J \in \mathbb{N}$ ), and (iv) number of snapshots used in the empirical computation of the reduced basis ( $N \in \mathbb{N}$ ). To this end, we note that the error itself can be split into the following contributions

$$(3.1) \quad \begin{aligned} \left\| u - \mathbf{P}_{X_{h,s,N,J}^{(\text{rb})}} u_h \right\|_{L^2(\mathbb{U};X)}^2 &\lesssim \underbrace{\|u - u_h\|_{L^2(\mathbb{U};X)}^2}_{\text{Galerkin error}} \\ &+ \left( 1 + \underbrace{\left\| \mathbf{P}_{X_{h,s,N,J}^{(\text{rb})}} \right\|_{X_h \rightarrow X_{h,s,N,J}^{(\text{rb})}}^2}_{\leq 1} \right) \underbrace{\|u_h - u_h^{(s)}\|_{L^2(\mathbb{U};X)}^2}_{\text{Truncation Error}} \\ &+ \underbrace{\|u_h^{(s)} - \mathbf{P}_{X_{h,J}^{(\text{rb})}} u_h^{(s)}\|_{L^2(\mathbb{U};X)}^2}_{\text{POD Error}}, \end{aligned}$$

where for  $\mathbf{y} = (y_1, \dots, y_s, \dots) \in \mathbb{U}$  we set  $u_h^{(s)}(\mathbf{y}) = u_h(y_1, y_2, \dots, y_s, 0, 0, \dots)$ . The implicit constant in (3.1) is independent of  $h$ ,  $s$ ,  $N$ , and  $J$ .

To estimate the Galerkin error, we note that standard inf-sup theory yields the following estimate, which is valid pointwise for each  $\mathbf{y} \in \mathbb{U}$

$$(3.2) \quad \|u(\mathbf{y}) - u_h(\mathbf{y})\|_X \leq \left( 1 + \frac{\bar{\alpha}}{\underline{\alpha}} \right) \inf_{v_h \in X_h} \|u(\mathbf{y}) - v_h\|_X$$

and by exploiting that  $\mathbb{U}$  has unit measure we obtain

$$(3.3) \quad \begin{aligned} \|u - u_h\|_{L^2(\mathbb{U};X)} &\leq \|u - u_h\|_{L^\infty(\mathbb{U};X)} \\ &\leq \left( 1 + \frac{\bar{\alpha}}{\underline{\alpha}} \right) \sup_{\mathbf{y} \in \mathbb{U}} \inf_{v_h \in X_h} \|u(\mathbf{y}) - v_h\|_X. \end{aligned}$$

To estimate the truncation error, we exploit again that  $\mathbb{U}$  has unit measure and that the  $(\mathbf{b}, p, \varepsilon)$ -holomorphy of  $u_h$  yields

$$(3.4) \quad \left\| u_h - u_h^{(s)} \right\|_{L^\infty(\mathbb{U}; X)} \lesssim s^{-(1/p-1)},$$

with the constant depending only on  $p \in (0, 1)$  and  $\mathbf{b}$ , see, e.g., [19, Theorem 2.1]. It thus remains to bound the POD error.

**3.2. POD Sampling Error.** To estimate the POD error, we note that

$$(3.5) \quad \left\| u_h^{(s)} - \mathbf{P}_{X_{h,s,N,J}^{(\text{rb})}} u_h^{(s)} \right\|_{L^2(\mathbb{U}; X)}^2 = \int_{\mathbb{U}^{(s)}} \left\| u_h^{(s)}(\mathbf{y}) - \mathbf{P}_{X_{h,s,N,J}^{(\text{rb})}} u_h^{(s)}(\mathbf{y}) \right\|_X^2 \mu^s(d\mathbf{y}),$$

and that (2.31) is obtained by applying an equal weights,  $N$ -points quadrature rule with points  $\{\mathbf{y}^{(n)}\}_{n=1}^N \subset \mathbb{U}^{(s)}$ ,  $s \in \mathbb{N}$  to (3.5). As we show in the following, quasi-Monte Carlo and higher-order quasi-Monte Carlo estimates, such as the Halton sequence or the IPL sequences, see Appendix B for details, are now immediately applicable.

LEMMA 3.1. *It holds*

$$(3.6) \quad \left| \left\| u_h^{(s)} - \mathbf{P}_{X_{h,s,N,J}^{(\text{rb})}} u_h^{(s)} \right\|_{L^2(\mathbb{U}^{(s)}; X)}^2 - \varepsilon_{h,s,N,J} \left( X_{h,s,N,J}^{(\text{rb})} \right) \right| \lesssim N^{-\alpha}.$$

Here, we obtain  $\alpha = 1 - \delta$  for any  $\delta \in (0, 1)$  for the the Halton sequence under the assumption  $p \in (0, \frac{1}{3})$  and  $\alpha = \frac{1}{p}$  for the IPL sequences. In the former case, the implicit constant in (3.6) depends on  $\delta$ , and tends to infinity as  $\delta \rightarrow 1^+$ .

*Proof.* Under the assumptions established in Subsection 2.3, the map  $\mathbb{U} \ni \mathbf{y} \mapsto u_h(\mathbf{y}) \in X$  is  $(\mathbf{b}, p, \varepsilon)$ -holomorphic and continuous. Next, it follows from Lemma A.1 that the map

$$(3.7) \quad \mathbb{U} \ni \mathbf{y} \mapsto \left\| u_h(\mathbf{y}) - \mathbf{P}_{X_{h,s,N,J}^{(\text{rb})}} u_h(\mathbf{y}) \right\|_X^2 \in \mathbb{R}.$$

is so as well. Using this, the result of this lemma is a direct consequence of Lemmas B.1 and B.2 in Appendix B for the Halton and HoQMC quadrature rules, respectively.  $\square$

Using (3.3), (3.4), and (3.6) to bound the errors in (3.1) implies the following error bound.

COROLLARY 3.2. *It holds*

$$(3.8) \quad \left\| u - \mathbf{P}_{X_{h,s,N,J}^{(\text{rb})}} u_h \right\|_{L^2(\mathbb{U}; X)}^2 \lesssim \sup_{\mathbf{y} \in \mathbb{U}} \inf_{v_h \in X_h} \|u(\mathbf{y}) - v_h\|_X^2 + s^{-2(1/p-1)} + N^{-\alpha} + \varepsilon_{h,s,N,J} \left( X_{h,s,N,J}^{(\text{rb})} \right),$$

with  $\alpha = 1 - \delta$  in case of the Halton sequence under the assumption  $p \in (0, \frac{1}{3})$  and  $\alpha = \frac{1}{p}$  in case of the IPL sequences for  $p \in (0, 1)$ . In the former case, the hidden constant in (3.8) tends to infinity as  $\delta \rightarrow 1^+$ .

We note that  $\varepsilon_{h,s,N} \left( X_{h,s,N,J}^{(\text{rb})} \right)$  can be fully controlled a-posteriori during computations by selecting an appropriately dimension  $J$  for the POD space in (2.39). In the following, we give an a-priori analysis of this term.

**3.3. A-priori analysis of the POD error.** Considering

$$(3.9) \quad \varepsilon_{h,s,N} \left( X_{N,s,h,J}^{(\text{rb})} \right) = \sum_{i=J+1}^r \sigma_{h,i}^2$$

as given in (2.39) we observe that it is fully determined by the eigenvalues  $\sigma_{h,i}^2$  of the matrix  $\mathbf{C} = \frac{1}{N} \tilde{\mathbf{S}}^* \mathbf{M}_h \tilde{\mathbf{S}}$ , see also Remark 1. In the following, we bound  $\varepsilon_{h,s,N} \left( X_{h,s,N,J}^{(\text{rb})} \right)$  in terms of  $N$  and  $J$ .

LEMMA 3.3. *It holds*

$$(3.10) \quad \varepsilon_{h,s,N} \left( X_{h,s,N,J}^{(\text{rb})} \right) \lesssim N^{-\alpha} + J^{-2(1/p-1)}$$

with the same considerations as stated in Corollary 3.2 for  $\alpha$  and the hidden constant in (3.10).

*Proof.* We observe that  $\mathbf{C}_h = \frac{1}{N} \tilde{\mathbf{S}}^* \mathbf{M} \tilde{\mathbf{S}}$  in (2.40),  $\frac{1}{N} (\mathbf{M}_h^*)^{1/2} \tilde{\mathbf{S}}^* \tilde{\mathbf{S}} \mathbf{M}_h^{1/2}$ , and  $\mathbf{K} = \frac{1}{N} \tilde{\mathbf{S}}^* \tilde{\mathbf{S}} \mathbf{M}_h$  have the very same eigenvalues  $\sigma_{h,i}^2$  and that the latter,  $\mathbf{K}$ , is the matrix representation of

$$(3.11) \quad \mathbf{K}_{h,s,N} w_h = \frac{1}{N} \sum_{n=1}^N u_h(\mathbf{y}^{(n)}) \left( u_h(\mathbf{y}^{(n)}), w_h \right)_X,$$

which also has eigenvalues  $\sigma_{h,i}^2$ . Using this notation, and recalling (2.25), we estimate

$$(3.12) \quad \begin{aligned} \varepsilon_{h,s,N} \left( X_{h,s,N,J}^{(\text{rb})} \right) &= \sum_{i=J+1}^r \sigma_{h,i}^2 \\ &= \min_{\substack{\mathbf{v} \in \mathbb{C}^{N_h \times J} \\ \mathbf{v}^* \mathbf{v} = \mathbf{I}}} \text{trace}(\mathbf{v}^* \mathbf{C} \mathbf{v}) \\ &= \min_{\substack{V \subset X_h \\ \dim V \leq J}} \text{trace}(\mathbf{P}_V \mathbf{K}_{h,s,N} \mathbf{P}_V) \\ &= \min_{\substack{V \subset X_h \\ \dim V \leq J}} \left( \text{trace}(\mathbf{P}_V \mathbf{K}_{h,s,N} \mathbf{P}_V - \mathbf{P}_V \mathbf{K}_h \mathbf{P}_V) + \text{trace}(\mathbf{P}_V \mathbf{K}_h \mathbf{P}_V) \right) \end{aligned}$$

where, for an arbitrary orthonormal basis  $\{\chi_i\}_{i=1}^{N_h}$  of  $X_h$ , it holds

$$(3.13) \quad \begin{aligned} &\text{trace}(\mathbf{P}_V \mathbf{K}_{h,s,N} \mathbf{P}_V - \mathbf{P}_V \mathbf{K}_h \mathbf{P}_V) \\ &= \sum_{i=1}^{N_h} \left( (\mathbf{K}_{h,s,N} - \mathbf{K}_h) \mathbf{P}_V \chi_i, \mathbf{P}_V \chi_i \right)_X \\ &= \sum_{i=1}^{N_h} \left( \mathbf{K}_{h,s,N} \mathbf{P}_V \chi_i, \mathbf{P}_V \chi_i \right)_X - \sum_{i=1}^{N_h} \left( \mathbf{K}_h \mathbf{P}_V \chi_i, \mathbf{P}_V \chi_i \right)_X \\ &= \frac{1}{N} \sum_{n=1}^N \sum_{i=1}^{N_h} \left( \mathbf{P}_V u_h(\mathbf{y}^{(n)}), \chi_i \right)_X^2 - \int_{\mathbb{U}^{(s)}} \sum_{i=1}^{N_h} \left( \mathbf{P}_V u_h(\mathbf{y}), \chi_i \right)_X^2 d\mu^{(s)}(\mathbf{y}) \\ &= \frac{1}{N} \sum_{n=1}^N \left\| \mathbf{P}_V u_h(\mathbf{y}^{(n)}) \right\|_X^2 - \int_{\mathbb{U}^{(s)}} \left\| \mathbf{P}_V u_h(\mathbf{y}) \right\|_X^2 d\mu^{(s)}(\mathbf{y}) \\ &\lesssim N^{-\alpha}. \end{aligned}$$

This implies

$$(3.14) \quad \varepsilon_{h,s,N} \left( X_{h,s,N,J}^{(\text{rb})} \right) \lesssim N^{-\alpha} + \underbrace{\min_{\substack{V \subset X_h \\ \dim V \leq J}} \text{trace}(\mathbf{K}_h|_V)}_{=\varepsilon_h(X_{h,J}^{(\text{rb})})},$$

where the last term can be estimated using (2.29), implying the assertion.  $\square$

COROLLARY 3.4. *It holds*

$$(3.15) \quad \left\| u - \mathbf{P}_{X_{h,s,N,J}^{(\text{rb})}} u_h \right\|_{L^2(\mathbb{U};X)} \lesssim \sup_{\mathbf{y} \in \mathbb{U}} \inf_{v_h \in X_h} \|u(\mathbf{y}) - v_h\|_X + s^{-(1/p-1)} + N^{-\alpha/2} + J^{-(1/p-1)}$$

with the same considerations stated in Corollary 3.2 for  $\alpha$  and for the hidden constant in (3.15).

*Proof.* Combine Corollary 3.2 and Lemma 3.3.  $\square$

Balancing errors yields the following a-priori estimate for the ranks of the POD generated subspace  $X_{h,s,N,J}^{(\text{rb})} \subset X_h$ .

COROLLARY 3.5. *Choosing  $J$  in (3.9) such that*

$$(3.16) \quad \varepsilon_{h,s,N} \left( X_{h,s,N,J}^{(\text{rb})} \right) \lesssim N^{-\alpha}$$

yields a POD subspace  $X_{h,s,N,J}^{(\text{rb})} \subset X_h$  with dimension at most  $J \sim N^{\frac{\alpha}{2(1/p-1)}}$  and satisfying

$$(3.17) \quad \left\| u - \mathbf{P}_{X_{h,s,N,J}^{(\text{rb})}} u_h \right\|_{L^2(\mathbb{U};X)} \lesssim \sup_{\mathbf{y} \in \mathbb{U}} \inf_{v_h \in X_h} \|u(\mathbf{y}) - v_h\|_X + s^{-(1/p-1)} + N^{-\alpha/2}.$$

**4. Fully Discrete Error Analysis of the Galerkin-POD NN.** In this section, we discuss the approximation properties of the Galerkin-POD NN. We are interested in a fully discrete error analysis for the approximation of the parameter-to-solution map by means of NNs by taking into account all the previously discussed error sources.

**4.1. Artificial Neural Networks.** Let  $L \in \mathbb{N}$ ,  $\ell_0, \dots, \ell_L \in \mathbb{N}$  and let  $\sigma : \mathbb{R} \rightarrow \mathbb{R}$  be a nonlinear function, referred to in the following as the *activation function*. Set

$$(4.1) \quad \Theta := \prod_{k=1}^L \left( \mathbb{R}^{\ell_k \times \ell_{k-1}} \times \mathbb{R}^{\ell_k} \right).$$

For  $\boldsymbol{\theta} = (\boldsymbol{\theta}_1, \dots, \boldsymbol{\theta}_L) \in \Theta$ , with  $\boldsymbol{\theta}_k = (\mathbf{W}_k, \mathbf{b}_k)$ ,  $\mathbf{W}_k \in \mathbb{R}^{\ell_k \times \ell_{k-1}}$ ,  $\mathbf{b}_k \in \mathbb{R}^{\ell_k}$ , consider the affine transformation  $\mathbf{A}_k : \mathbb{R}^{\ell_{k-1}} \rightarrow \mathbb{R}^{\ell_k} : \mathbf{x} \mapsto \mathbf{W}_k \mathbf{x} + \mathbf{b}_k$  for  $k \in \{1, \dots, L\}$ . We define a *neural network (NN)* with activation function  $\sigma$  as the map  $\Psi_{\boldsymbol{\theta}} : \mathbb{R}^{\ell_0} \rightarrow \mathbb{R}^{\ell_L}$  defined as

$$(4.2) \quad \Psi_{\boldsymbol{\theta}}(\mathbf{x}) := \begin{cases} \mathbf{A}_1(\mathbf{x}), & L = 1, \\ (\mathbf{A}_L \circ \sigma \circ \mathbf{A}_{L-1} \circ \sigma \cdots \circ \sigma \circ \mathbf{A}_1)(\mathbf{x}), & L \geq 2, \end{cases}$$

where the activation function  $\sigma : \mathbb{R} \rightarrow \mathbb{R}$  is applied componentwise. We define the depth and the width of an NN as

$$(4.3) \quad \text{width}(\Psi_{\boldsymbol{\theta}}) = \max\{\ell_0, \dots, \ell_L\} \quad \text{and} \quad \text{depth}(\Psi_{\boldsymbol{\theta}}) = L + 1,$$

respectively.

In the present work, we consider as activation function the hyperbolic tangent

$$(4.4) \quad \sigma(x) = \tanh(x) = \frac{\exp(x) - \exp(-x)}{\exp(x) + \exp(-x)},$$

however other options are possible.

When this particular function is used, we refer to (4.2) as a tanh NN. In the following,  $\mathcal{NN}_{D,W,\ell_0,\ell_D}$  corresponds to the set of all NNs with input dimension  $\ell_0$ , output dimension  $\ell_D$ , a width of at most  $W$ , and a depth of at most  $D$  layers.

**4.2. Galerkin-POD NN Architecture.** Let  $\{\zeta_1^{(\text{rb})}, \dots, \zeta_J^{(\text{rb})}\}$  correspond to the basis for the finite dimensional space  $X_{h,s,N,J}^{(\text{rb})}$  constructed in (2.38) and  $u_h(\mathbf{y})$  the solution to (2.16). Then the map

$$(4.5) \quad \boldsymbol{\pi}_{h,J}^{(\text{rb})} : \mathbb{U} \rightarrow \mathbb{C}^J : \mathbf{y} \mapsto \begin{pmatrix} \left( u_h(\mathbf{y}), \zeta_1^{(\text{rb})} \right)_X \\ \vdots \\ \left( u_h(\mathbf{y}), \zeta_J^{(\text{rb})} \right)_X \end{pmatrix}$$

gathers the coefficients of the projection of  $u_h(\mathbf{y})$  onto the subspace  $X_{h,s,N,J}^{(\text{rb})}$ , i.e. of  $\mathbb{P}_{X_{h,s,N,J}^{(\text{rb})}} u_h(\mathbf{y})$ , for each  $\mathbf{y} \in \mathbb{U}$ . Unfortunately, as the setting under consideration makes use of complex-valued Hilbert spaces, the map introduced in (4.5) is complex-valued and we cannot readily use NNs as defined in subsection 4.1. To alleviate this, and as described in [63, Section 4.2], we consider instead the mapping

$$(4.6) \quad \boldsymbol{\pi}_{h,J,\mathbb{R}}^{(\text{rb})} : \mathbb{U} \rightarrow \mathbb{R}^{2J} : \mathbf{y} \mapsto \begin{pmatrix} \boldsymbol{\alpha}^{\Re}(\mathbf{y}) \\ \boldsymbol{\alpha}^{\Im}(\mathbf{y}) \end{pmatrix} := \begin{pmatrix} \Re \left\{ \boldsymbol{\pi}_{h,J}^{(\text{rb})}(\mathbf{y}) \right\} \\ \Im \left\{ \boldsymbol{\pi}_{h,J}^{(\text{rb})}(\mathbf{y}) \right\} \end{pmatrix} \in \mathbb{R}^{2J}, \quad \mathbf{y} \in \mathbb{U},$$

which approximates the real and imaginary parts of the output in (4.5) separately. We observe that the maps

$$(4.7) \quad \mathcal{A}^{\Re} : \mathbb{U} \rightarrow \mathbb{R}^J : \mathbf{y} \mapsto \boldsymbol{\alpha}^{\Re}(\mathbf{y}) \quad \text{and} \quad \mathcal{A}^{\Im} : \mathbb{U} \rightarrow \mathbb{R}^J : \mathbf{y} \mapsto \boldsymbol{\alpha}^{\Im}(\mathbf{y})$$

are  $(\mathbf{b}, p, \varepsilon)$ -holomorphic as consequence of [22, Lemma A.1], thus rendering (4.6) so as well.

For the approximation of  $\boldsymbol{\pi}_{h,J,\mathbb{R}}^{(\text{rb})}$  we seek a tanh NN  $\boldsymbol{\pi}_{\boldsymbol{\theta}}^{(\text{rb})} \in \mathcal{NN}_{D,W,s,2J}$  with  $\boldsymbol{\theta} \in \Theta$ , i.e. with  $s \in \mathbb{N}$  inputs (one for each component of the parametric input  $\mathbf{y} \in \mathbb{U}^{(s)}$ ),  $2J$  outputs accounting for the  $J$  complex reduced coefficients, and depth and width  $D$  and  $W$ , respectively. The first  $J$  outputs of this NN are denoted as  $\boldsymbol{\alpha}_{\boldsymbol{\theta}}^{\Re}(\mathbf{y})$ , whereas the last  $J$  by  $\boldsymbol{\alpha}_{\boldsymbol{\theta}}^{\Im}(\mathbf{y})$ . These are intended to approximate the maps defined in (4.7). We refer to Figure 4.1 for an illustration of this architecture.

For a given  $\boldsymbol{\theta} \in \Theta$ , the reconstruction of  $\boldsymbol{\pi}_{\boldsymbol{\theta}}^{(\text{rb})}$  through the basis  $\zeta_1^{(\text{rb})}, \dots, \zeta_J^{(\text{rb})}$  of  $X_{h,s,N,J}^{(\text{rb})}$  is given by

$$(4.8) \quad u_{J,\boldsymbol{\theta}}^{(\text{rb},\mathcal{NN})}(\mathbf{y}) = \sum_{j=1}^J (\boldsymbol{\alpha}_{j,\boldsymbol{\theta}}^{\Re}(\mathbf{y}) + i\boldsymbol{\alpha}_{j,\boldsymbol{\theta}}^{\Im}(\mathbf{y})) (\mathbf{y}) \zeta_j^{(\text{rb})}, \quad \mathbf{y} \in \mathbb{U}^{(s)},$$

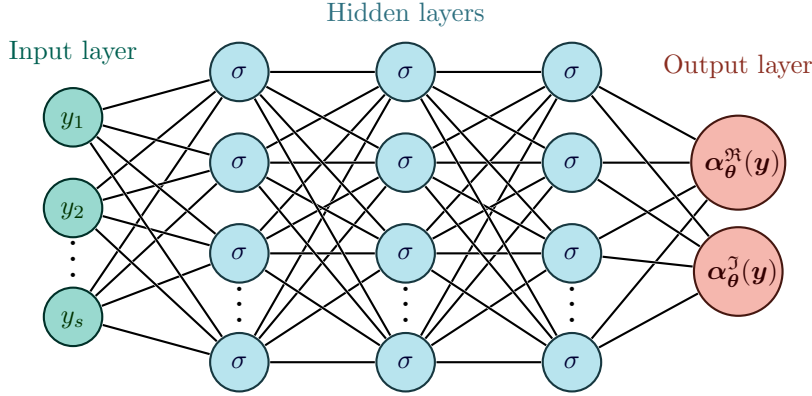


Fig. 4.1: NN architecture for the approximation of the map  $\pi_{h,J}^{(\text{rb})} : \mathbb{U} \rightarrow \mathbb{C}^J$  with the NN  $\pi_{\theta}^{(\text{rb})} : \mathbb{U}^{(s)} \rightarrow \mathbb{R}^{2J}$ . The NN accepts  $s \in \mathbb{N}$  inputs in the input layer corresponding to the components of the parametric input  $\mathbf{y} = (y_1, \dots, y_s) \in \mathbb{U}^{(s)}$ . In addition, there are  $2J$  outputs for the approximation of both the real and imaginary parts, i.e.  $\alpha_{\theta}^{\Re}(\mathbf{y})$  and  $\alpha_{\theta}^{\Im}(\mathbf{y})$ , respectively, of the reduced coefficients.

where for  $\mathbf{y} \in \mathbb{U}^{(s)}$

$$(4.9) \quad \alpha_{\theta}^{\Re}(\mathbf{y}) := \begin{pmatrix} \alpha_{1,\theta}^{\Re}(\mathbf{y}) \\ \vdots \\ \alpha_{J,\theta}^{\Re}(\mathbf{y}) \end{pmatrix} \in \mathbb{R}^J \quad \text{and} \quad \alpha_{\theta}^{\Im}(\mathbf{y}) := \begin{pmatrix} \alpha_{1,\theta}^{\Im}(\mathbf{y}) \\ \vdots \\ \alpha_{J,\theta}^{\Im}(\mathbf{y}) \end{pmatrix} \in \mathbb{R}^J.$$

**4.3. Fully Discrete Error Analysis.** We present a fully discrete analysis of the Galerkin-POD NN algorithm based on the results introduced in [Section 3](#).

For a given  $s \in \mathbb{N}$ , we set

$$(4.10) \quad \mathcal{T}_s : \mathbb{U} \rightarrow \mathbb{U}^{(s)} : (y_1, \dots, y_s, y_{s+1}, \dots) \mapsto (y_1, \dots, y_s).$$

LEMMA 4.1. *Assume that  $\mathbf{b} \in \ell^p(\mathbb{N})$  is strictly decreasing. For each  $n \in \mathbb{N}$ ,  $n \geq s$ , there exists a tanh NN  $\pi_n^{(\text{rb})} \in \mathcal{NN}_{D,W,s,2J}$  and  $C > 0$  such that*

$$(4.11) \quad \left\| \pi_{J,\mathbb{R}}^{(\text{rb})} - \pi_n^{(\text{rb})} \circ \mathcal{T}_s \right\|_{L^2(\mathbb{U}; \mathbb{R}^{2J})} \lesssim Jn^{-(1/p-1/2)} + s^{-(1/p-1)}$$

with  $D = \mathcal{O}(\log_2(n))$  and  $W = \mathcal{O}(n^2)$ .

*Proof.* This result follows from [\[22, Lemma 5.7\]](#), which in turn uses tools from [\[1\]](#), and [\(3.4\)](#).  $\square$

Equipped with this result, together with the results presented in [Section 3](#), we may state the following error bound.

THEOREM 4.2. *Assume that  $\mathbf{b} \in \ell^p(\mathbb{N})$  is strictly decreasing. Then there exists  $\pi_n^{(\text{rb})} \in \mathcal{NN}_{D,W,s,2J}$  such that*

$$(4.12) \quad \left\| u - \mathcal{R} \left( \pi_n^{(\text{rb})} \right) \circ \mathcal{T}_s \right\|_{L^2(\mathbb{U}; X)} \lesssim \sup_{\mathbf{y} \in \mathbb{U}} \inf_{v_h \in X_h} \|u(\mathbf{y}) - v_h\|_X + Jn^{-(1/p-1/2)} + s^{-(1/p-1)} + N^{-\frac{\alpha}{2}} + J^{-(1/p-1)}.$$

with  $W = \mathcal{O}(n^2)$  and  $D = \mathcal{O}(\log_2(n))$ , where for a  $\tanh$  NN  $\Psi$  with  $s$  inputs and  $2J$  outputs, the reconstruction operator  $\mathcal{R}$  is defined as

$$(4.13) \quad \mathcal{R}(\Psi)(\mathbf{y}) = \sum_{i=1}^J ((\Psi(\mathbf{y}))_i + \iota(\Psi(\mathbf{y}))_{i+J}) \zeta_i^{(\text{rb})}, \quad \mathbf{y} \in \mathbb{U}^{(s)}.$$

*Proof.* Let  $\pi_n^{(\text{rb})}$  be as in [Lemma 4.1](#). It follows from the application of the triangle inequality that

$$(4.14) \quad \left\| u_h - \mathcal{R}(\pi_{\mathcal{NN}}^{(\text{rb})}) \circ \mathcal{T}_s \right\|_{L^2(\mathbb{U}; X)} \leq \underbrace{\left\| u_h - \mathbb{P}_{X_{h,J}^{(\text{rb})}} u_h \right\|_{L^2(\mathbb{U}; X)}}_{(\spadesuit)} + \underbrace{\left\| \mathbb{P}_{X_{h,J}^{(\text{rb})}} u_h - \mathcal{R}(\pi_{\mathcal{NN}}^{(\text{rb})}) \circ \mathcal{T}_s \right\|_{L^2(\mathbb{U}; X)}}_{(\clubsuit)}.$$

The term  $(\spadesuit)$  is bounded according to [Corollary 3.4](#). We proceed to bound  $(\clubsuit)$ . Recalling that  $\zeta_1^{(\text{rb})}, \dots, \zeta_J^{(\text{rb})}$  is an orthonormal basis of  $X_{h,J}^{(\text{rb})}$  with respect to the inner product of  $X$  one may readily observe that

$$(4.15) \quad \left\| \mathbb{P}_{X_{h,J}^{(\text{rb})}} u_h - \mathcal{R}(\pi^{(\text{rb})}) \circ \mathcal{T}_s \right\|_{L^2(\mathbb{U}; X)} = \left\| \pi_{J, \mathbb{R}}^{(\text{rb})} - \pi_{\theta}^{(\text{rb})} \circ \mathcal{T}_s \right\|_{L^2(\mathbb{U}; \mathbb{R}^{2J})}.$$

The application of [Lemma 4.1](#) to bound [\(4.15\)](#) yields the assertion.  $\square$

Equilibrating approximation errors yields a-priori requirements for the neural network parameters to maintain the approximation rates of the quasi-Monte Carlo sampling.

**COROLLARY 4.3.** *Assume that  $\mathbf{b} \in \ell^p(\mathbb{N})$  is strictly decreasing. Select  $J$  as in [Corollary 3.5](#) and  $n \sim N^{\frac{\alpha p}{(1-p)(2-p)}}$ . Then there exists a  $\tanh$  NN  $\pi_n^{(\text{rb})} \in \mathcal{NN}_{D,W,s,2J}$  of depth  $D = \mathcal{O}(\log_2(n))$  and width  $W = \mathcal{O}(n^2)$  such that*

$$(4.16) \quad \left\| u - \mathcal{R}(\pi_n^{(\text{rb})}) \circ \mathcal{T}_s \right\|_{L^2(\mathbb{U}; X)} \lesssim \sup_{\mathbf{y} \in \mathbb{U}} \inf_{v_h \in X_h} \|u(\mathbf{y}) - v_h\|_X + s^{-(1/p-1)} + N^{-\frac{\alpha}{2}}.$$

**4.4. Neural Network Training.** Having proven the existence of NN with good approximation properties it remains to comment on how to find it, commonly referred to as *training*. To this end, given a data set consisting in  $N$  training inputs  $\mathbf{y}^{(i)} \in \mathbb{U}^{(s)}$ ,  $i = 1, \dots, N$ , and the corresponding high-fidelity snapshots  $u_h(\mathbf{y}^{(i)})$ ,  $i = 1, \dots, N$ , the idea is to adjust the parameters  $\theta$  such that a loss functional is minimized. On the continuous level, a natural candidate is the error measure [\(2.31\)](#) from the POD framework which, by coincidence, is exactly the mean square error (MSE). Then, due to the orthogonality of the POD bases, the MSE loss is given by

$$(4.17) \quad L_{\text{MSE}}(\theta) := \frac{1}{N} \sum_{i=1}^N \left\| \left( \pi_{J, \mathbb{R}}^{(\text{rb})} \circ \mathcal{T}_s \right) \left( \mathbf{y}^{(i)} \right) - \pi_{\theta}^{(\text{rb})} \left( \mathbf{y}^{(i)} \right) \right\|_{\mathbb{R}^{2J}}^2.$$

The latter is one of the most common choices for NN training.

**5. Application: Sound-soft Acoustic Scattering.** We consider a concrete application that fits the framework of [Subsection 2.3](#), i.e. the scattering by a parametrically defined sound-soft object in three spatial dimensions. The following section recapitulates the notation and main result of [\[22\]](#).

**5.1. Parametrized Domain Deformations.** Let  $\hat{D} \subset \mathbb{R}^3$  be a bounded reference domain with Lipschitz boundary  $\hat{\Gamma} = \partial\hat{D}$  and set  $\mathbf{r}_{\mathbf{y}}: \hat{\Gamma} \rightarrow \mathbb{R}^3$  with

$$(5.1) \quad \mathbf{r}_{\mathbf{y}}(\hat{\mathbf{x}}) = \varphi_0(\hat{\mathbf{x}}) + \sum_{j \geq 1} y_j \varphi_j(\hat{\mathbf{x}}), \quad \hat{\mathbf{x}} \in \hat{\Gamma}, \quad \mathbf{y} = (y_j)_{j \geq 1} \in \mathbb{U},$$

and  $\varphi_j: \hat{\Gamma} \rightarrow \mathbb{R}^3$  for  $j \in \mathbb{N}$ . This gives rise to a collection of parametric boundaries  $\{\Gamma_{\mathbf{y}}\}_{\mathbf{y} \in \mathbb{U}}$  of the form

$$(5.2) \quad \Gamma_{\mathbf{y}} := \{\mathbf{x} \in \mathbb{R}^3 : \mathbf{x} = \mathbf{r}_{\mathbf{y}}(\hat{\mathbf{x}}), \quad \hat{\mathbf{x}} \in \hat{\Gamma}\},$$

In the following, we work under the assumptions stated below.

ASSUMPTION 5.1. *Let  $\hat{\Gamma}$  be the reference Lipschitz boundary.*

1. *The functions  $(\varphi_i)_{i \in \mathbb{N}} \subset \mathcal{C}^{0,1}(\hat{\Gamma}; \mathbb{R}^3)$  are such that for each  $\mathbf{y} \in \mathbb{U}$  one has that  $\mathbf{r}_{\mathbf{y}}: \hat{\Gamma} \rightarrow \Gamma_{\mathbf{y}}$  is bijective and bi-Lipschitz, and  $\Gamma_{\mathbf{y}}$  is the boundary of a Lipschitz domain.*
2. *There exists  $p \in (0, 1)$  such that  $\mathbf{b} := \left( \|\varphi_j\|_{\mathcal{C}^{0,1}(\hat{\Gamma}, \mathbb{R}^3)} \right)_{j \in \mathbb{N}} \in \ell^p(\mathbb{N})$ .*
3. *There is a decomposition  $\mathcal{G}$  of  $\hat{\Gamma}$  such that for each  $\mathbf{y} \in \mathbb{U}$  and each  $\tau \in \mathcal{G}$  one has that  $\mathbf{r}_{\mathbf{y}} \circ \chi_{\tau} \in \mathcal{C}^{1,1}(\bar{\tau}; \mathbb{R}^3)$ .*

**Item 1** and **Item 3** of the assumption guarantee that all parametric boundaries  $\Gamma_{\mathbf{y}}$  are Lipschitz and piecewise  $\mathcal{C}^{1,1}$ . Thus, since the topological properties of  $\hat{\Gamma}$  and  $\Gamma_{\mathbf{y}}$  coincide,  $\Gamma_{\mathbf{y}}$  gives rise to parametrized domains  $D_{\mathbf{y}}$  which have the same topological properties as  $\hat{D}$ . Moreover, **Item 2** implies absolute convergence of (5.1) as an element of  $\mathcal{C}^{0,1}$ . A further consequence is that the pullback operator, defined as  $\tau_{\mathbf{y}}\varphi := \varphi \circ \mathbf{r}_{\mathbf{y}} \in L^2(\hat{\Gamma})$ , for each  $\mathbf{y} \in \mathbb{U}$  and  $\varphi \in L^2(\Gamma_{\mathbf{y}})$  in an isomorphism, i.e.,  $\tau_{\mathbf{y}} \in \mathcal{L}_{\text{iso}}\left(L^2(\Gamma_{\mathbf{y}}), L^2(\hat{\Gamma})\right)$  for each  $\mathbf{y} \in \mathbb{U}$ , see, e.g. [22, Lemma 2.13].

**5.2. Application: Sound-Soft Acoustic Scattering.** In the following, we denote by  $D_{\mathbf{y}} \subset \mathbb{R}^3$  the domain enclosed by  $\Gamma_{\mathbf{y}}$  and by  $D_{\mathbf{y}}^c =: \mathbb{R}^3 \setminus \overline{D_{\mathbf{y}}}$  the corresponding exterior domain.

Provided a wavenumber  $\kappa > 0$  and an incident direction  $\hat{\mathbf{d}}_{\text{inc}} \in \mathbb{S}^2 := \{\mathbf{x} \in \mathbb{R}^3 : \|\mathbf{x}\| = 1\}$ , we define an incident plane wave  $u^{\text{inc}}(\mathbf{x}) := \exp(i\kappa\mathbf{x} \cdot \hat{\mathbf{d}}_{\text{inc}})$ . The aim is then to find the sound-soft scattered wave  $u_{\mathbf{y}}^{\text{scat}} \in H_{\text{loc}}^1(D^c)$  such that the total field  $u_{\mathbf{y}} := u^{\text{inc}} + u_{\mathbf{y}}^{\text{scat}}$  satisfies

$$(5.3a) \quad \Delta u_{\mathbf{y}} + \kappa^2 u_{\mathbf{y}} = 0, \quad \text{in } D_{\mathbf{y}}^c,$$

$$(5.3b) \quad u_{\mathbf{y}} = 0, \quad \text{on } \Gamma_{\mathbf{y}},$$

and the scattered field additionally satisfies the Sommerfeld radiation condition

$$(5.4) \quad \frac{\partial u_{\mathbf{y}}^{\text{scat}}}{\partial r}(\mathbf{x}) - i\kappa u_{\mathbf{y}}^{\text{scat}}(\mathbf{x}) = o(r^{-1})$$

as  $r := \|\mathbf{x}\| \rightarrow \infty$ , uniformly in  $\hat{\mathbf{x}} := \mathbf{x}/r$ . Thus, since  $u^{\text{inc}}$  satisfies (5.3a) on its own, (5.3) can be cast as follows: find  $u_{\mathbf{y}}^{\text{scat}} \in H_{\text{loc}}^1(D^c)$  such that

$$(5.5a) \quad \Delta u_{\mathbf{y}}^{\text{scat}} + \kappa^2 u_{\mathbf{y}}^{\text{scat}} = 0, \quad \text{in } D_{\mathbf{y}}^c,$$

$$(5.5b) \quad u_{\mathbf{y}}^{\text{scat}} = -u^{\text{inc}}, \quad \text{on } \Gamma_{\mathbf{y}},$$

and (5.4) holds. Equation (5.5) has a unique solution, which may be obtained in terms of a boundary integral formulation as outlined in the following.



**5.3. Boundary Integral Formulation.** Standard results yield the following representation for the scattered field  $u_{\mathbf{y}}^{\text{scat}} : D_{\mathbf{y}}^c \rightarrow \mathbb{C}$  in terms of the unknown Neumann datum

$$(5.6) \quad u_{\mathbf{y}}^{\text{scat}}(\mathbf{x}) = -\mathcal{S}_{\Gamma_{\mathbf{y}}}^{(\kappa)} \left( \frac{\partial u_{\mathbf{y}}}{\partial \mathbf{n}_{\Gamma_{\mathbf{y}}}} \right) (\mathbf{x}), \quad \mathbf{x} \in D_{\mathbf{y}}^c,$$

with  $\mathcal{S}_{\Gamma_{\mathbf{y}}}^{(\kappa)} : H^{-\frac{1}{2}}(\Gamma_{\mathbf{y}}) \rightarrow H_{\text{loc}}^1(\Delta, D_{\mathbf{y}}^c)$  being the acoustic single layer potential (for further details we refer to [58]). Define

$$(5.7) \quad \gamma_{\Gamma_{\mathbf{y}}}^c : H_{\text{loc}}^1(D_{\mathbf{y}}^c) \rightarrow H^{\frac{1}{2}}(\Gamma_{\mathbf{y}}) \quad \text{and} \quad \frac{\partial}{\partial \mathbf{n}_{\Gamma_{\mathbf{y}}}} : H^1(\Delta, D_{\mathbf{y}}^c) \rightarrow H^{-\frac{1}{2}}(\Gamma_{\mathbf{y}})$$

which applied to (5.6) yield

$$(5.8a) \quad \mathcal{V}_{\Gamma_{\mathbf{y}}}^{(\kappa)} \frac{\partial u_{\mathbf{y}}}{\partial \mathbf{n}_{\Gamma_{\mathbf{y}}}} = \gamma_{\Gamma_{\mathbf{y}}}^c u_{\mathbf{y}}^{\text{inc}}, \quad \text{and } \Gamma_{\mathbf{y}}, \quad \text{and,}$$

$$(5.8b) \quad \left( \frac{1}{2} \text{Id} + \mathcal{K}_{\Gamma_{\mathbf{y}}}^{(\kappa)'} \right) \frac{\partial u_{\mathbf{y}}}{\partial \mathbf{n}_{\Gamma_{\mathbf{y}}}} = \frac{\partial u_{\mathbf{y}}^{\text{inc}}}{\partial \mathbf{n}_{\Gamma_{\mathbf{y}}}}, \quad \text{on } \Gamma_{\mathbf{y}},$$

with the single layer operator

$$(5.9) \quad \mathcal{V}_{\Gamma_{\mathbf{y}}}^{(\kappa)} := \gamma_{\Gamma_{\mathbf{y}}}^c \mathcal{S}_{\Gamma_{\mathbf{y}}}^{(\kappa)} : H^{-\frac{1}{2}}(\Gamma_{\mathbf{y}}) \rightarrow H^{\frac{1}{2}}(\Gamma_{\mathbf{y}}),$$

and the adjoint double layer operator

$$(5.10) \quad \frac{1}{2} \text{Id} + \mathcal{K}_{\Gamma_{\mathbf{y}}}^{(\kappa)'} := \frac{\partial}{\partial \mathbf{n}_{\Gamma_{\mathbf{y}}}} \mathcal{S}_{\Gamma_{\mathbf{y}}}^{(\kappa)} : H^{-\frac{1}{2}}(\Gamma_{\mathbf{y}}) \rightarrow H^{-\frac{1}{2}}(\Gamma_{\mathbf{y}}).$$

**5.4. Combined Boundary Integral Formulation.** Given a *coupling parameter*  $\eta \in \mathbb{R} \setminus \{0\}$  we combine (5.8a) and (5.8b) to define

$$(5.11) \quad \mathcal{A}_{\Gamma_{\mathbf{y}}}^{(\kappa, \eta)'} := \frac{1}{2} \text{Id} + \mathcal{K}_{\Gamma_{\mathbf{y}}}^{(\kappa)'} - \eta \mathcal{V}_{\Gamma_{\mathbf{y}}}^{(\kappa)}.$$

Exploiting that  $\phi_{\mathbf{y}} := \frac{\partial u_{\mathbf{y}}}{\partial \mathbf{n}_{\Gamma_{\mathbf{y}}}} \in L^2(\Gamma_{\mathbf{y}})$ , see, e.g., [50], a new boundary integral approach to (5.3a) is to solve for  $\phi_{\mathbf{y}} \in L^2(\Gamma_{\mathbf{y}})$  such that

$$(5.12) \quad \mathcal{A}_{\Gamma_{\mathbf{y}}}^{(\kappa, \eta)'} \phi_{\mathbf{y}} = f_{\mathbf{y}} := \frac{\partial u_{\mathbf{y}}^{\text{inc}}}{\partial \mathbf{n}_{\Gamma_{\mathbf{y}}}} - \eta \gamma_{\Gamma_{\mathbf{y}}}^c u_{\mathbf{y}}^{\text{inc}} \in L^2(\Gamma_{\mathbf{y}}).$$

The operator  $\mathcal{A}_{\Gamma_{\mathbf{y}}}^{(\kappa, \eta)'} : L^2(\Gamma_{\mathbf{y}}) \rightarrow L^2(\Gamma_{\mathbf{y}})$  is a boundedly invertible and continuous linear operator for any  $\kappa \in \mathbb{R}_+$ , unlike the first and second kind BIEs (5.8a) and (5.8b), respectively, further rendering (5.12) well-posed in  $L^2(\Gamma_{\mathbf{y}})$ . We recall that the *parameter-to-solution map*

$$(5.13) \quad \mathbb{U} \rightarrow L^2(\hat{\Gamma}) : \mathbf{y} \mapsto \hat{\phi}_{\mathbf{y}} := \tau_{\mathbf{y}}(\phi_{\mathbf{y}}),$$

the *parameter-to-operator map*

$$(5.14) \quad \mathbb{U} \rightarrow \mathcal{L} \left( L^2(\hat{\Gamma}), L^2(\hat{\Gamma}) \right) : \mathbf{y} \mapsto \hat{\mathcal{A}}_{\mathbf{y}}^{(\kappa, \eta)'} := \tau_{\mathbf{y}} \mathcal{A}_{\Gamma_{\mathbf{y}}}^{(\kappa, \eta)'} \tau_{\mathbf{y}}^{-1},$$

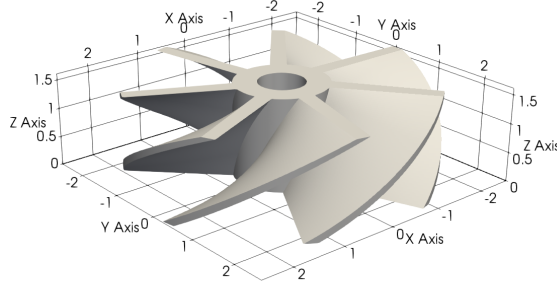


Fig. 6.1: The turbine geometry which is randomly deformed.

and the *parameter-to-inverse-operator map*

$$(5.15) \quad \mathbb{U} \rightarrow \mathcal{L} \left( L^2(\hat{\Gamma}), L^2(\hat{\Gamma}) \right) : \mathbf{y} \mapsto \left( \hat{\mathbf{A}}_{\mathbf{y}}^{(\kappa, \eta)'} \right)^{-1} = \tau_{\mathbf{y}} \left( \mathbf{A}_{\Gamma_{\mathbf{y}}}^{(\kappa, \eta)'} \right)^{-1} \tau_{\mathbf{y}}^{-1},$$

are  $(\mathbf{b}, p, \varepsilon)$ -holomorphic and continuous if [Assumption 5.1](#) is satisfied, see [\[22, Lemma 2.4.2 and Corollaries 4.7 and 4.8\]](#). Thus, setting  $X = L^2(\hat{\Gamma})$ , and

$$(5.16) \quad \mathbf{a}(u, v; \mathbf{y}) = \left( \hat{\mathbf{A}}_{\mathbf{y}}^{(\kappa, \eta)'} u, v \right)_{L^2(\hat{\Gamma})} \in B(L^2(\hat{\Gamma})),$$

$$(5.17) \quad \mathbf{f}(v; \mathbf{y}) = (\tau_{\mathbf{y}} f_{\mathbf{y}}, v)_{L^2(\hat{\Gamma})} \in L^2(\hat{\Gamma})',$$

$\widehat{\phi}_{\mathbf{y}}$  is a solution to [\(2.12\)](#) with  $\mathbf{a}$  and  $\mathbf{f}$  satisfying [\(2.13\)](#), [\(2.14\)](#), and [\(2.15\)](#). Moreover, for a sequence of finite-dimensional subspaces of one parameter  $\{\widehat{X}_h\}_{h>0} \subset L^2(\hat{\Gamma})$  that are densely embedded in  $L^2(\hat{\Gamma})$ , one can show that the discrete inf-sup condition [\(2.17\)](#) holds for all  $h \leq h_0$  see, e.g., [\[40\]](#). Thus, all the derived results in [section 3](#) and [section 4](#) apply to this case, in particular [Corollary 3.5](#) and [Corollary 4.3](#).

**REMARK 2.** *Although here we rely on the results from [\[22\]](#), one can certainly extend these results to boundary integral formulations for open arcs following [\[54\]](#), two-dimensional boundary integral operators in fractional Sobolev spaces as in [\[31, 32, 13\]](#), and boundary integral formulations for time-dependent parabolic problems [\[12\]](#).*

**REMARK 3.** *In the computational implementation of [\(5.16\)](#) and [\(5.17\)](#), one may choose to define subspaces  $X_{h, \mathbf{y}} = \tau_{\mathbf{y}}^{-1} \widehat{X}_h \subset L^2(\Gamma_{\mathbf{y}})$  for which [Assumption 5.1](#) yields a parameter-dependent sequence of one-parameter finite-dimensional subspaces which are densely embedded in  $L^2(\Gamma_{\mathbf{y}})$ . The computations can then be carried out in the physical domain by using readily available software packages with a subsequent pullback of the solution to the reference domain.*

## 6. Numerical Experiments.

**6.1. Model problem.** For the numerical experiments, we consider the sound-soft acoustic scattering problem posed on three-dimensional parametric Lipschitz boundaries, exactly as discussed in [section 5](#). Our goal is to learn the corresponding parameter-to-solution map [\(5.13\)](#) following [subsection 4.2](#).

To this end, we choose our reference boundary  $\hat{\Gamma}$  to be the three-dimensional turbine geometry portrayed in [Figure 6.1](#). For the domain deformations  $\mathbf{r}_{\mathbf{y}} : \hat{\Gamma} \rightarrow \mathbb{R}^3$

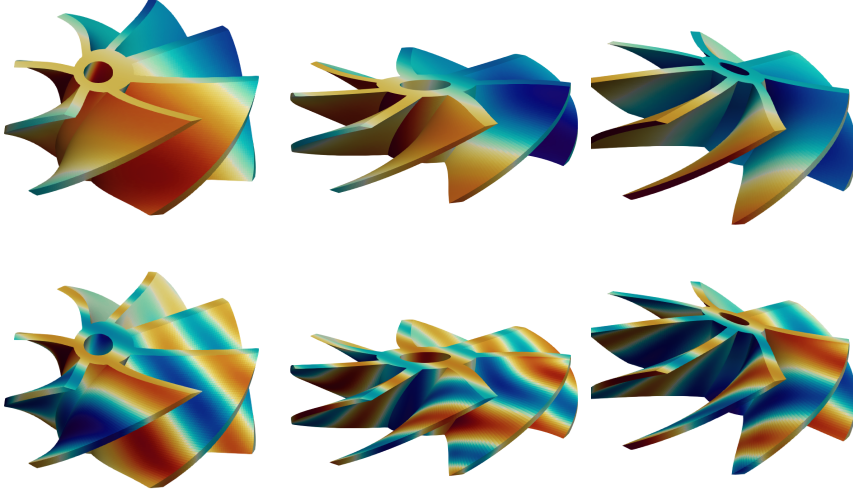


Fig. 6.2: Realizations of the randomly deformed domain. Colors illustrate the real part of the values of the parameter-to-solution map given by (5.12) for the wavenumbers  $\kappa = 1$  (top) and  $\kappa = 4$  (bottom).

we choose (5.1) with  $\varphi_0(\hat{\mathbf{x}}) = \hat{\mathbf{x}}$  and  $\varphi_i(\hat{\mathbf{x}}) = \sqrt{\lambda_k} \chi_k(\hat{\mathbf{x}})$ ,  $k \in \mathbb{N}$ , where  $(\lambda_k, \chi_k)$  are the eigenpairs of the covariance operator  $\mathcal{C}: [L^2(\hat{\Gamma})]^3 \rightarrow [L^2(\hat{\Gamma})]^3$  given by

$$(6.1) \quad (\mathcal{C}\mathbf{u})(\hat{\mathbf{x}}) := \int_{\hat{\Gamma}} \text{Cov}[\mathbf{r}](\hat{\mathbf{x}}, \hat{\mathbf{y}}) \mathbf{u}(\hat{\mathbf{y}}) d\sigma_{\hat{\mathbf{y}}}$$

with

$$\text{Cov}[\mathbf{r}](\hat{\mathbf{x}}, \hat{\mathbf{y}}) = \begin{pmatrix} \frac{4}{5} K_{7/2} \left( \frac{2\|\hat{\mathbf{x}} - \hat{\mathbf{y}}\|_2}{3} \right) & \frac{1}{10} K_{7/2} \left( \frac{\|\hat{\mathbf{x}} - \hat{\mathbf{y}}\|_2}{8} \right) & 0 \\ \frac{1}{10} K_{7/2} \left( \frac{\|\hat{\mathbf{x}} - \hat{\mathbf{y}}\|_2}{8} \right) & \frac{2}{5} K_{7/2} \left( \frac{\|\hat{\mathbf{x}} - \hat{\mathbf{y}}\|_2}{6} \right) & 0 \\ 0 & 0 & \frac{2}{10} K_{7/2} \left( \frac{\|\hat{\mathbf{x}} - \hat{\mathbf{y}}\|_2}{24} \right) \end{pmatrix}.$$

Here,  $K_{7/2}: \mathbb{R}_{>0} \rightarrow \mathbb{R}_{>0}$  refers to the Matérn 7/2-kernel, which is given as

$$K_{7/2}(r) = \left( 1 + 3r + \frac{27r^2}{7} + \frac{18r^3}{7} + \frac{27r^4}{35} \right) e^{-3r}.$$

A few examples of parametrized domain boundaries generated by these domain deformations are shown in Figure 6.2. The decay of the eigenvalues of the covariance operator (6.1) is depicted in Figure 6.3.

**6.2. Implementation and computational setup.** For the generation of the samples we pursue a black-box approach based on the C++ open source software library BEMBEL, see [21], which is able to perform the required computations within the isogeometric setting [10, 20]. For the generation of the training and test samples we rely on Halton points, implying  $\alpha = 1 - \delta$  for any  $\delta > 0$  in Corollary 4.3. The sampling process is accelerated by a hybrid MPI and OpenMP parallelization, where each

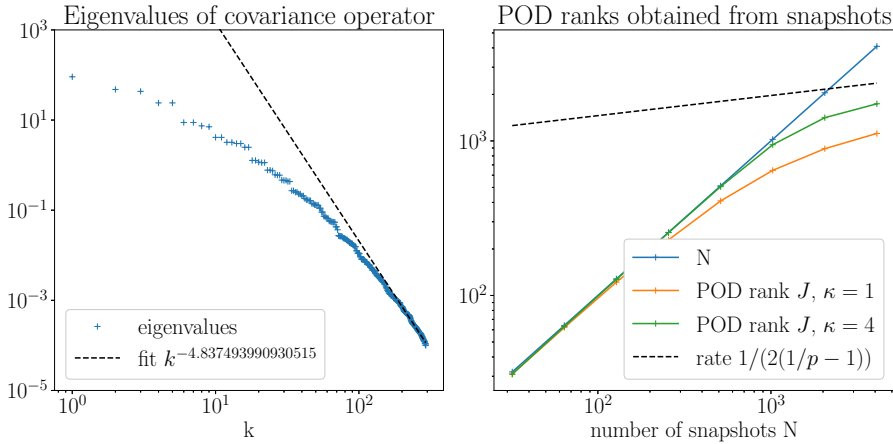


Fig. 6.3: Decay of the eigenvalues of the covariance operator (6.1) used to generate the domain deformations (left) and resulting POD-ranks for wavenumbers  $\kappa = 1$  and  $\kappa = 4$  (right).

sample is accelerated using `OpenMP`, and the sampling process is accelerated using `MPI`. The sampling process is performed on 16 nodes of a cluster with each node being equipped with two Intel Xeon “Sapphire Rapids” 48-core processors with 2.10GHz frequency, making 1’536 cores in total, and one `MPI` process per node. Once the samples are generated, we perform all remaining computations within `Python` using the `scipy` package for linear algebra and the `PyTorch` package for the neural network computations. For the minimization of the loss functional we use the `Adam` optimizer implemented in the `PyTorch` package. The computations using `PyTorch` are carried out on a `NVIDIA A100` GPU with 40GB RAM.

**6.3. Sampling.** In the following we focus ourselves on the empirical verification of the a-priori bound of the POD rank from [Corollary 3.5](#) and the combined Galerkin-POD NN error estimate from [Corollary 4.3](#) in the asymptotics in the number of samples  $N$ . The asymptotic behavior in the Galerkin error and the truncation error for the encoder have been well investigated in the literature and a study in these parameters is computationally out of reach at the time of writing this article. Thus, in the following we fix those discretizations. For the domain deformations we use second order, globally continuous B-splines with a total of 4116 degrees of freedom. Following [\[28\]](#), using an incomplete pivoted Cholesky decomposition with a tolerance of  $10^{-4}$  balances the truncation error with the discretization error, and we obtain a truncated approximate expansion (5.1) with 293 terms, i.e.,  $s = 293$ . For the solution of the boundary integral equations we employ second order B-splines with 5376 degrees of freedom and a direct solver. Following these choices, we generate  $2^{13} = 8192$  samples for the wavenumbers  $\kappa = 1$  and  $\kappa = 4$ . For each wavenumber this takes about 8.5 hours on the 16 nodes of the above mentioned cluster. We will use the first half of these samples for our numerical studies and the second half to measure the  $NN$ -generalization error.

**6.4. POD-ranks.** We determine the POD-reduced basis by truncating the SVD of the snapshot matrix with respect to the Euclidean inner product such that the

error in the Frobenius norm is below a certain tolerance  $\tau$ . In accordance with [Corollary 3.2](#), this tolerance needs to be asymptotically comparable to the Galerkin error, the truncation error for the decoder, and the sampling error of the quasi Monte Carlo sampling. We thus choose  $\tau = \frac{1}{100\sqrt{N}}$ . The resulting POD-ranks are illustrated in [Figure 6.3](#) and confirm the a-priori bound from [Corollary 3.5](#).

**6.5. Neural network convergence.** It remains to verify the convergence estimate from [Corollary 4.3](#). To this end, inspired by [Corollary 4.3](#), we choose a tanh NN with depth  $\max\{1, \log_2(n)\} + 2$  and width  $n^2$  with  $n = N^{\frac{p}{(1-p)(2-p)}}$  and  $p = 2/4.8$ , cf. [Figure 6.3](#). As learning rate we choose  $10^{-3} \cdot L_{\text{MSE}}$ , with  $L_{\text{MSE}}$  being the current value of the loss function as defined in [\(4.17\)](#). We use the standard settings of the Adam optimizer otherwise and stop the iteration when  $L_{\text{MSE}} < \frac{1}{N}$ , when the iteration stagnates, or when  $10^7$  iterations have been performed. We say that the iteration stagnates if, the values of  $L_{\text{MSE}}$  fluctuate in a relative range of  $10^{-5}$  for  $10^3$  iterations or if there is a relative increase of its value of at least  $10^{-3}$  compared to the last  $10^3$  iterations. To further stabilize and accelerate the training process we employ BatchNormalization, cf. [\[38\]](#), as provided by the PyTorch package. The results are illustrated [Figure 6.4](#) and confirm the theoretically predicted convergence rates from [Corollary 4.3](#) for  $\kappa = 1$ . For the more challenging  $\kappa = 4$  case, our optimization procedure could not reach the training error aimed for, and optimization stagnated. Still, the observed convergence rates indicate the validity of our a-priori analysis. We expect that an improved training procedure leading to smaller training errors will improve the observed convergence behaviour in  $N$ .

**7. Concluding Remarks.** In this work, we consider the problem of approximation the parameter-to-solution map associated to parameter-dependent variational problems using the so-called Galerkin POD-NN method [\[36\]](#). We present a fully discrete error analysis accounting for a variety of error sources in the construction of a basis of reduced order by means of the Galerkin POD and discuss how this translates in their approximation using NNs in the Galerkin POD-NN. The analysis is applicable to a rather general class of variational problems and yields a-priori estimates on the POD ranks and NN parameters in terms of parametric regularity. Our numerical examples for three dimensional wave scattering demonstrate that our analysis is applicable to black-box implementations where obtaining the training samples is achieved by a specialized software package and POD and NN computations can be done with standard tools in Python. A remaining issue for practical applications is the NN training. In fact, we experienced stagnating optimization processes during training as the main obstacle in our numerical examples. Still, we could observe that if loss functional reached the desired training accuracy, we always reached the convergence rates predicted by our theory. Current and future work encompasses the use of multi-level NN strategies as the one proposed in [\[30\]](#), together with extension to time-dependent problems and electromagnetic wave scattering.

**Data availability.** The snapshot data and the Python code for the POD and training of the NN will be made publicly available upon acceptance of this article.

**Acknowledgements.** The authors appreciate access to the Marvin cluster of the University of Bonn and the support of the Deutsche Forschungsgemeinschaft (DFG, German Research Foundation) under Germany’s Excellence Strategy – GZ 2047/1, Projekt-ID 390685813 – and project 501419255.

FH’s work was funded by the Deutsche Forschungsgemeinschaft (DFG, German Research Foundation) Project-ID 258734477 SFB 1173 and the Austrian Science

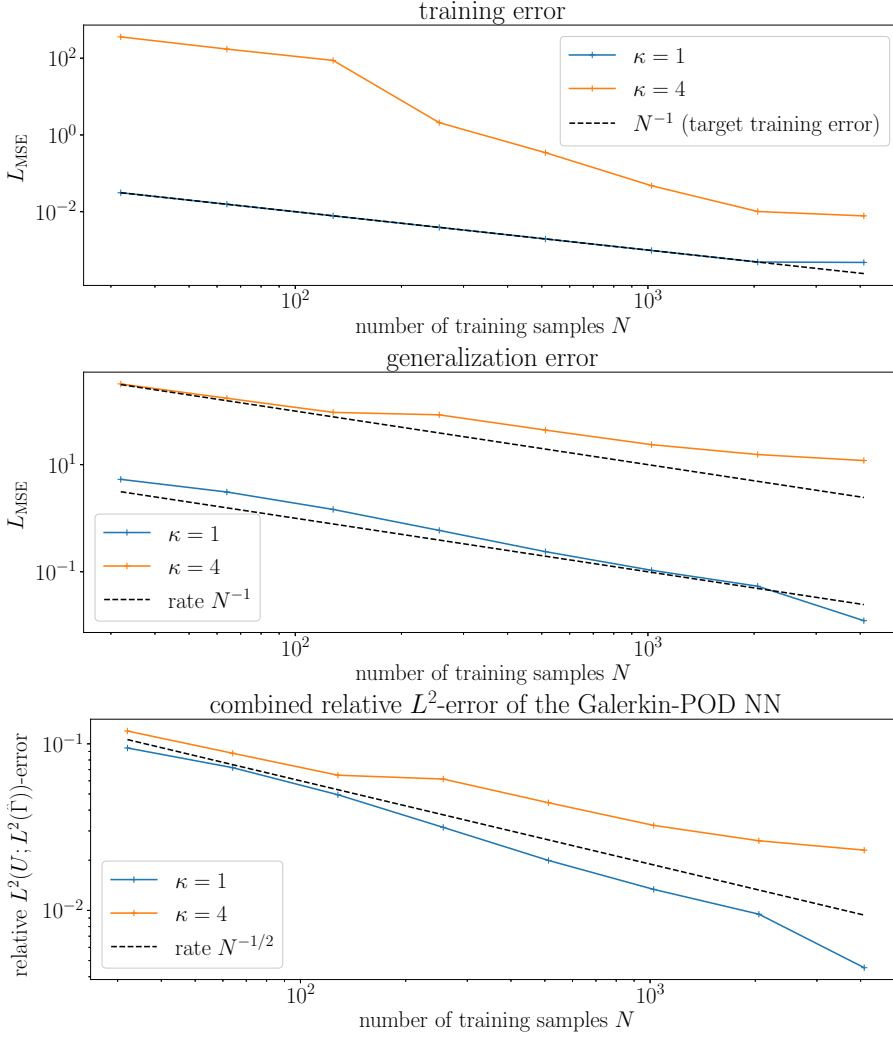


Fig. 6.4: Training (top) and generalization errors (middle) for the Galerkin-POD neural network approximation. The combined  $L^2(\mathbb{U}; L^2(\hat{\Gamma}))$ -error of the Galerkin-POD NN is shown at the bottom and confirms the theoretical estimate from [Corollary 4.3](#).

Fund (FWF) under the project I6667-N. Funding was also received from the European Research Council (ERC) under the Horizon 2020 research and innovation program of the European Union (Grant agreement No. 101125225).

### Appendix A. Auxiliary Results.

LEMMA A.1. *Let  $X$  be a complex Hilbert space equipped with the inner product  $(\cdot, \cdot)_X$  and induced norm  $\|\cdot\|_X$ . Let  $\mathbb{U} \ni \mathbf{y} \mapsto f(\mathbf{y}) \in X$  be  $(\mathbf{b}, p, \varepsilon)$ -holomorphic and continuous continuous map when  $\mathbb{U}$  is equipped with the product topology. Then the map*

$$(A.1) \quad \mathbb{U} \ni \mathbf{y} \mapsto \|f(\mathbf{y})\|_X^2 \in \mathbb{R}$$

is  $(\mathbf{b}, p, \varepsilon)$ -holomorphic and continuous with the same  $\mathbf{b} \in \ell^p(\mathbb{N})$ ,  $p \in (0, 1)$ , and  $\varepsilon > 0$ .

*Proof.* We proceed to verify [Definition 2.1](#) item-by-item. Firstly, one can readily verify that the uniform boundedness of the map introduced in [\(A.1\)](#).

Let  $\boldsymbol{\rho} := (\rho_j)_{j \geq 1}$  be any  $(\mathbf{b}, p, \varepsilon)$ -admissible sequence of numbers of numbers strictly larger than one. We consider the complex extension of [\(A.1\)](#) to  $\mathcal{O}_{\boldsymbol{\rho}}$  given by

$$(A.2) \quad \mathcal{O}_{\boldsymbol{\rho}} \ni \mathbf{z} \mapsto g(\mathbf{z}) := (f(\mathbf{z}), f(\bar{\mathbf{z}}))_X.$$

Observe that this extension is well-defined for each  $\mathbf{z} \in \mathcal{O}_{\boldsymbol{\rho}}$  since this straightforwardly implies  $\bar{\mathbf{z}} \in \mathcal{O}_{\boldsymbol{\rho}}$ .

Computing the complex derivative of  $g(\mathbf{z})$  for  $\mathbf{z} \in \mathcal{O}_{\boldsymbol{\rho}}$  we obtain

$$(A.3) \quad \begin{aligned} \frac{dg}{dz_j}(\mathbf{z}) &= \lim_{|h| \rightarrow 0^+} \frac{(f(\mathbf{z} + h\mathbf{e}_j), f(\overline{\mathbf{z} + h\mathbf{e}_j}))_X - (f(\mathbf{z}), f(\bar{\mathbf{z}}))_X}{h} \\ &= \lim_{|h| \rightarrow 0^+} \frac{(f(\mathbf{z} + h\mathbf{e}_j), f(\overline{\mathbf{z} + h\mathbf{e}_j}))_X - (f(\mathbf{z}), f(\overline{\mathbf{z} + h\mathbf{e}_j}))_X}{h} \\ &\quad + \lim_{|h| \rightarrow 0^+} \frac{(f(\mathbf{z}), f(\overline{\mathbf{z} + h\mathbf{e}_j}))_X - (f(\mathbf{z}), f(\bar{\mathbf{z}}))_X}{h} \\ &= \lim_{|h| \rightarrow 0^+} \left( \frac{f(\mathbf{z} + h\mathbf{e}_j) - f(\mathbf{z})}{h}, f(\overline{\mathbf{z} + h\mathbf{e}_j}) \right)_X \\ &\quad + \lim_{|h| \rightarrow 0^+} \left( f(\mathbf{z}), \frac{f(\overline{\mathbf{z} + h\mathbf{e}_j}) - f(\bar{\mathbf{z}})}{\bar{h}} \right)_X. \end{aligned}$$

Exploiting the continuity of the inner product in each argument and that it is anti-linear in the second argument, yields

$$(A.4) \quad \begin{aligned} \frac{dg}{dz_j}(\mathbf{z}) &= \left( \lim_{|h| \rightarrow 0^+} \frac{f(\mathbf{z} + h\mathbf{e}_j) - f(\mathbf{z})}{h}, f(\bar{\mathbf{z}}) \right)_X \\ &\quad + \left( f(\mathbf{z}), \lim_{|h| \rightarrow 0^+} \frac{f(\overline{\mathbf{z} + h\mathbf{e}_j}) - f(\bar{\mathbf{z}})}{\bar{h}} \right)_X. \end{aligned}$$

Observing that

$$(A.5) \quad \lim_{|h| \rightarrow 0^+} \frac{f(\overline{\mathbf{z} + h\mathbf{e}_j}) - f(\bar{\mathbf{z}})}{\bar{h}} = \lim_{|h| \rightarrow 0^+} \frac{f(\bar{\mathbf{z}} + h\mathbf{e}_j) - f(\bar{\mathbf{z}})}{h} = \frac{df}{dz_j}(\bar{\mathbf{z}}),$$

implies

$$(A.6) \quad \frac{dg}{dz_j}(\mathbf{z}) = \left( \frac{df}{dz_j}(\mathbf{z}), f(\bar{\mathbf{z}}) \right)_X + \left( f(\mathbf{z}), \frac{df}{dz_j}(\bar{\mathbf{z}}) \right)_X, \quad \mathbf{z} \in \mathcal{O}_{\boldsymbol{\rho}}.$$

Observe that, similarly as with [\(A.2\)](#), the expression in [\(A.5\)](#) is well-defined for any  $\mathbf{z} \in \mathcal{O}_{\boldsymbol{\rho}}$  since this implies  $\bar{\mathbf{z}} \in \mathcal{O}_{\boldsymbol{\rho}}$ .  $\square$

### Appendix B. Quasi-Monte Carlo Integration.

Aiming to compute integrals of the kind

$$(B.1) \quad \mathcal{I}(f) = \int_{\mathbb{U}} f(\mathbf{y}) \mu(d\mathbf{y}),$$

for continuous  $f: \mathbb{U} \rightarrow \mathbb{R}$ , we perform a domain truncation from infinite dimensions to the finite dimensional setting. To this end, let  $s \in \mathbb{N}$  be the truncation dimension and set  $\mathbb{U}^{(s)} := [-1, 1]^s$ . This allows to approximate (B.1) by a numerical approximation of an integral over  $\mathbb{U}^{(s)}$  of the form

$$(B.2) \quad \mathcal{I}^{(s)}(f) := \int_{\mathbb{U}^{(s)}} f(\mathbf{y}) \mu^{(s)}(d\mathbf{y}),$$

where  $f^{(s)}: \mathbb{U}^{(s)} \rightarrow \mathbb{R}$  and  $f^{(s)}(y_1, \dots, y_s) = f(y_1, \dots, y_s, 0, \dots)$ . One of the most common ways to evaluate the integral are Monte Carlo-type quadrature rules with equal weights weights of the form

$$(B.3) \quad \mathcal{Q}^{(N,s)}(f) := \frac{1}{N} \sum_{n=1}^N f\left(2\mathbf{y}^{(n)} - 1\right),$$

where  $f(2\mathbf{y}^{(n)} - 1)$  corresponds to the evaluation of the integrand in sampling points  $\{\mathbf{y}^{(0)}, \dots, \mathbf{y}^{(N-1)}\} \subset [0, 1]^s$ . Although plain vanilla Monte Carlo methods are well known to lead to slow convergence in the root mean square sense, quasi-Monte Carlo methods provide faster and rigorous convergence rates for  $(\mathbf{b}, p, \varepsilon)$ -holomorphic integrands. In the following, we recall approximation estimates for the Halton sequence and IPL sequences.

LEMMA B.1 (Adaption of [29, Lemma 7]). *Assume that  $\mathbb{U} \ni \mathbf{y} \mapsto f(\mathbf{y}) \in \mathbb{R}$  is  $(\mathbf{b}, p, \varepsilon)$ -holomorphic for some  $\mathbf{b} \in \ell^p(\mathbb{N})$ ,  $p \in (0, \frac{1}{3})$ , and assume that the sample points in (B.3) are drawn according to the Halton sequence. Then*

$$\left| \mathcal{I}^{(s)}(f) - \mathcal{Q}^{(N,s)}(f) \right| \leq C(\delta) N^{\delta-1},$$

where  $C(\delta) \rightarrow \infty$  as  $\delta \rightarrow 0$ .

As explained previously, IPL rules have been proved to deliver convergence rates that are independent of the underlying parametric dimension, provided that the integrand satisfies specific parametric regularity estimate. The following result addresses this issue.

LEMMA B.2 ([18, Theorem 3.1]). *For  $m \geq 1$  and a prime  $b$ , let  $N = b^m$  denote the number of HoQMC points. Let  $s \geq 1$  and  $\boldsymbol{\beta} = \{\beta_j\}_{j \in \mathbb{N}}$  be a positive number sequence, and let  $\boldsymbol{\beta}_s = \{\beta_j\}_{j=1}^s$  denote the first  $s$  terms. Assume that  $\boldsymbol{\beta} \in \ell^p(\mathbb{N})$  for some  $p \in (0, 1)$ . If there exists  $c > 0$  such that a function  $F$  satisfies for  $\alpha := \left\lfloor \frac{1}{p} \right\rfloor + 1$  that*

$$(B.4) \quad \left| (\partial_{\mathbf{y}}^{\boldsymbol{\nu}} F)(\mathbf{y}) \right| \leq c |\boldsymbol{\nu}|! \boldsymbol{\beta}_s^{\boldsymbol{\nu}}, \quad \text{for all } \boldsymbol{\nu} \in \{0, 1, \dots, \alpha\}^s, \quad s \in \mathbb{N},$$

then the interlaced polynomial lattice rule of order  $\alpha$  with  $N$  points can be constructed in

$$(B.5) \quad \mathcal{O}(\alpha s N \log N + \alpha^2 s^2 N)$$

operations, such that for the quadrature error holds

$$(B.6) \quad \left| \mathcal{I}^{(s)}(f) - \mathcal{Q}^{(N,s)}(f) \right| \leq C_{\alpha, \boldsymbol{\beta}, b, p} N^{-1/p}$$

where the constant  $C_{\alpha, \boldsymbol{\beta}, b, p} < \infty$  is independent of  $s$  and  $N$ .



## REFERENCES

- [1] B. ADCOCK, S. BRUGIAPAGLIA, N. DEXTER, AND S. MORAGA, *Near-optimal learning of Banach-valued, high-dimensional functions via deep neural networks*, Neural Networks, 181 (2025), p. 106761.
- [2] M. BARRAULT, Y. MADAY, N. C. NGUYEN, AND A. T. PATERA, *An empirical interpolation method: application to efficient reduced-basis discretization of partial differential equations*, Comptes Rendus Mathématique, 339 (2004), pp. 667–672.
- [3] K. BHATTACHARYA, B. HOSSEINI, N. B. KOVACHKI, AND A. M. STUART, *Model reduction and neural networks for parametric PDEs*, The SMAI journal of computational mathematics, 7 (2021), pp. 121–157.
- [4] B. BOHN, J. GARCKE, AND M. GRIEBEL, *Algorithmic Mathematics in Machine Learning*, Society for Industrial and Applied Mathematics, Philadelphia, 2024.
- [5] H. BÖLCSKEI, P. GROHS, G. KUTYNIOK, AND P. PETERSEN, *Optimal Approximation with Sparsely Connected Deep Neural Networks*, SIAM Journal on Mathematics of Data Science, 1 (2019), pp. 8–45.
- [6] S. CHATURANTABUT AND D. C. SORENSEN, *Nonlinear model reduction via discrete empirical interpolation*, SIAM Journal on Scientific Computing, 32 (2010), pp. 2737–2764.
- [7] A. CHKIFA, A. COHEN, AND C. SCHWAB, *Breaking the curse of dimensionality in sparse polynomial approximation of parametric PDEs*, Journal de Mathématiques Pures et Appliquées, 103 (2015), pp. 400–428.
- [8] A. COHEN AND R. DEVORE, *Approximation of high-dimensional parametric PDEs*, Acta Numerica, 24 (2015), pp. 1–159.
- [9] A. COHEN AND R. DEVORE, *Kolmogorov widths under holomorphic mappings*, IMA Journal of Numerical Analysis, 36 (2016), pp. 1–12.
- [10] J. A. COTTRELL, T. J. R. HUGHES, AND Y. BAZILEVS, *Isogeometric Analysis: Toward Integration of CAD and FEA*, Wiley Publishing, Hoboken, NJ, first ed., 2009.
- [11] G. CYBENKO, *Approximation by superpositions of a sigmoidal function*, Mathematics of Control, Signals, and Systems, 2 (1989), pp. 303–314.
- [12] M. DALLA RIVA AND P. LUZZINI, *Dependence of the layer heat potentials upon support perturbations*, arXiv e-prints, (2023), pp. arXiv-2303.
- [13] M. DALLA RIVA, P. LUZZINI, AND P. MUSOLINO, *Shape analyticity and singular perturbations for layer potential operators*, ESAIM: Mathematical Modelling and Numerical Analysis, 56 (2022), pp. 1889–1910.
- [14] T. DE RYCK, S. LANTHALER, AND S. MISHRA, *On the approximation of functions by tanh neural networks*, Neural Networks, 143 (2021), pp. 732–750.
- [15] T. DE RYCK AND S. MISHRA, *Generic bounds on the approximation error for physics-informed (and) operator learning*, Advances in Neural Information Processing Systems, 35 (2022), pp. 10945–10958.
- [16] R. DEVORE, B. HANIN, AND G. PETROVA, *Neural network approximation*, Acta Numerica, 30 (2021), pp. 327–444.
- [17] J. DICK, R. N. GANTNER, Q. T. LE GIA, AND C. SCHWAB, *Higher order Quasi-Monte Carlo integration for Bayesian estimation*, Computers and Mathematics with Applications, 77 (2019), pp. 144–172.
- [18] J. DICK, F. Y. KUO, Q. T. LE GIA, D. NUYENS, AND C. SCHWAB, *Higher order QMC Petrov-Galerkin discretization for affine parametric operator equations with random field inputs*, SIAM Journal on Numerical Analysis, 52 (2014), pp. 2676–2702.
- [19] J. DICK, Q. T. LE GIA, AND C. SCHWAB, *Higher Order Quasi-Monte Carlo Integration for Holomorphic, Parametric Operator Equations*, SIAM/ASA Journal on Uncertainty Quantification, 4 (2016), pp. 48–79.
- [20] J. DÖLZ, H. HARBRECHT, C. JEREZ-HANCKES, AND M. MULTERER, *Isogeometric Multilevel Quadrature for Forward and Inverse Random Acoustic Scattering*, Computer Methods in Applied Mechanics and Engineering, 388 (2022), p. 114242.
- [21] J. DÖLZ, H. HARBRECHT, S. KURZ, M. MULTERER, S. SCHÖPS, AND F. WOLF, *Bembel: The fast isogeometric boundary element C++ library for Laplace, Helmholtz, and electric wave equation*, SoftwareX, 11 (2020), p. 100476.
- [22] J. DÖLZ AND F. HENRÍQUEZ, *Parametric shape holomorphy of boundary integral operators with applications*, SIAM Journal on Mathematical Analysis, 56 (2024), pp. 6731–6767.
- [23] N. R. FRANCO, S. FRESCA, A. MANZONI, AND P. ZUNINO, *Approximation bounds for convolutional neural networks in operator learning*, Neural Networks, 161 (2023), pp. 129–141.
- [24] P. GROHS AND G. KUTYNIOK, eds., *Mathematical Aspects of Deep Learning*, Cambridge University Press, 1 ed., Dec. 2022.

- [25] J. GUIBAS, M. MARDANI, Z. LI, A. TAO, A. ANANDKUMAR, AND B. CATANZARO, *Adaptive fourier neural operators: Efficient token mixers for transformers*, arXiv preprint arXiv:2111.13587, (2021).
- [26] M. GUO AND J. S. HESTHAVEN, *Data-driven reduced order modeling for time-dependent problems*, Computer methods in applied mechanics and engineering, 345 (2019), pp. 75–99.
- [27] J. H. HALTON, *On the Efficiency of Certain Quasi-Random Sequences of Points in Evaluating Multi-Dimensional Integrals*, Numerische Mathematik, 2 (1960), pp. 84–90.
- [28] H. HARBRECHT, M. PETERS, AND M. SIEBENMORGEN, *Efficient approximation of random fields for numerical applications*, Numerical Linear Algebra with Applications, 22 (2015), pp. 596–617.
- [29] H. HARBRECHT, M. PETERS, AND M. SIEBENMORGEN, *Analysis of the domain mapping method for elliptic diffusion problems on random domains*, Numerische Mathematik, 134 (2016), pp. 823–856.
- [30] C. HEISS, I. GÜHRING, AND M. EIGEL, *A neural multilevel method for high-dimensional parametric pdes*, in The Symbiosis of Deep Learning and Differential Equations, 2021.
- [31] F. HENRÍQUEZ, *Shape Uncertainty Quantification in Acoustic Scattering*, PhD thesis, ETH Zurich, 2021.
- [32] F. HENRÍQUEZ AND C. SCHWAB, *Shape holomorphy of the Calderón projector for the Laplacian in  $\mathbb{R}^2$* , Integral Equations and Operator Theory, 93 (2021), p. 43.
- [33] L. HERRMANN, J. A. OPSCHOOR, AND C. SCHWAB, *Constructive deep ReLU neural network approximation*, Journal of Scientific Computing, 90 (2022), pp. 1–37.
- [34] L. HERRMANN, C. SCHWAB, AND J. ZECH, *Neural and spectral operator surrogates: unified construction and expression rate bounds*, Advances in Computational Mathematics, 50 (2024), p. 72.
- [35] J. S. HESTHAVEN, G. ROZZA, B. STAMM, ET AL., *Certified reduced basis methods for parametrized partial differential equations*, vol. 590, Springer, 2016.
- [36] J. S. HESTHAVEN AND S. UBBIALI, *Non-intrusive reduced order modeling of nonlinear problems using neural networks*, Journal of Computational Physics, 363 (2018), pp. 55–78.
- [37] K. HORNIK, *Approximation capabilities of multilayer feedforward networks*, Neural Networks, 4 (1991), pp. 251–257.
- [38] S. IOFFE AND C. SZEGEDY, *Batch Normalization: Accelerating Deep Network Training by Reducing Internal Covariate Shift*, Mar. 2015.
- [39] N. KOVACHKI, S. LANTHALER, AND S. MISHRA, *On universal approximation and error bounds for Fourier neural operators*, Journal of Machine Learning Research, 22 (2021), pp. 1–76.
- [40] R. KRESS, *Linear Integral Equations*, no. volume 82 in Applied Mathematical Sciences, Springer, New York, third edition ed., 2014.
- [41] S. LANTHALER, *Operator learning with PCA-Net: upper and lower complexity bounds*, Journal of Machine Learning Research, 24 (2023), pp. 1–67.
- [42] S. LANTHALER, S. MISHRA, AND G. E. KARNIADAKIS, *Error estimates for deepoanets: A deep learning framework in infinite dimensions*, Transactions of Mathematics and Its Applications, 6 (2022), p. tnac001.
- [43] S. LANTHALER, R. MOLINARO, P. HADORN, AND S. MISHRA, *Nonlinear reconstruction for operator learning of PDEs with discontinuities*, arXiv preprint arXiv:2210.01074, (2022).
- [44] Z. LI, N. KOVACHKI, K. AZIZZADENESHELI, B. LIU, K. BHATTACHARYA, A. STUART, AND A. ANANDKUMAR, *Fourier neural operator for parametric partial differential equations*, arXiv preprint arXiv:2010.08895, (2020).
- [45] M. LOËVE, *Probability Theory*, no. 46 in Graduate Texts in Mathematics, Springer, Berlin New York, 4th ed ed., 1978.
- [46] M. LONGO, S. MISHRA, T. K. RUSCH, AND C. SCHWAB, *Higher-Order Quasi-Monte Carlo Training of Deep Neural Networks*, SIAM Journal on Scientific Computing, 43 (2021), pp. A3938–A3966.
- [47] L. LU, P. JIN, G. PANG, Z. ZHANG, AND G. E. KARNIADAKIS, *Learning nonlinear operators via deepoanet based on the universal approximation theorem of operators*, Nature machine intelligence, 3 (2021), pp. 218–229.
- [48] K. O. LYE, S. MISHRA, AND D. RAY, *Deep learning observables in computational fluid dynamics*, Journal of Computational Physics, 410 (2020), p. 109339.
- [49] S. MISHRA AND T. K. RUSCH, *Enhancing Accuracy of Deep Learning Algorithms by Training with Low-Discrepancy Sequences*, SIAM Journal on Numerical Analysis, 59 (2021), pp. 1811–1834.
- [50] J. NEČAS, *Les méthodes directes en théorie des équations elliptiques*, Masson Academia, Paris Prague, 1967.
- [51] M. OHLBERGER AND S. RAVE, *Reduced basis methods: Success, limitations and future chal-*

- lenges, 2016.
- [52] P. PETERSEN AND F. VOIGTLAENDER, *Optimal approximation of piecewise smooth functions using deep ReLU neural networks*, *Neural Networks*, 108 (2018), pp. 296–330.
  - [53] F. PICHI, B. MOYA, AND J. S. HESTHAVEN, *A graph convolutional autoencoder approach to model order reduction for parametrized PDEs*, *Journal of Computational Physics*, 501 (2024), p. 112762.
  - [54] J. PINTO, F. HENRÍQUEZ, AND C. JEREZ-HANCKES, *Shape holomorphy of boundary integral operators on multiple open arcs*, *The Journal of Fourier Analysis and Applications* (Submitted), (2023).
  - [55] M. PRASTHOFER, T. DE RYCK, AND S. MISHRA, *Variable-input deep operator networks*, arXiv preprint arXiv:2205.11404, (2022).
  - [56] A. QUATERONI, A. MANZONI, AND F. NEGRI, *Reduced basis methods for partial differential equations*, vol. 92 of *Unitext*, Springer, Cham, 2016. An introduction, *La Matematica per il 3+2*.
  - [57] B. RAONIC, R. MOLINARO, T. ROHNER, S. MISHRA, AND E. DE BEZENAC, *Convolutional neural operators*, in *ICLR 2023 Workshop on Physics for Machine Learning*, 2023.
  - [58] S. SAUTER AND C. SCHWAB, *Boundary Element Methods*, Springer, Berlin, Heidelberg, 2010.
  - [59] C. SCHWAB AND J. ZECH, *Deep learning in high dimension: Neural network expression rates for generalized polynomial chaos expansions in UQ*, *Analysis and Applications*, 17 (2019), pp. 19–55.
  - [60] Q. WANG, J. S. HESTHAVEN, AND D. RAY, *Non-intrusive reduced order modeling of unsteady flows using artificial neural networks with application to a combustion problem*, *Journal of computational physics*, 384 (2019), pp. 289–307.
  - [61] Q. WANG, N. RIPAMONTI, AND J. S. HESTHAVEN, *Recurrent neural network closure of parametric POD-Galerkin reduced-order models based on the Mori-Zwanzig formalism*, *Journal of Computational Physics*, 410 (2020), p. 109402.
  - [62] S. WANG, H. WANG, AND P. PERDIKARIS, *Learning the solution operator of parametric partial differential equations with physics-informed DeepONets*, *Science advances*, 7 (2021), p. eabi8605.
  - [63] P. WEDER, M. KAST, F. HENRÍQUEZ, AND J. S. HESTHAVEN, *Galerkin Neural Network-POD for Acoustic and Electromagnetic Wave Propagation in Parametric Domains*, arXiv preprint arXiv:2406.13567, (2024).